

JGR Atmospheres

RESEARCH ARTICLE

10.1029/2021JD035824

Special Section:

The land-air coupling over Tibetan Plateau and its global climate effects

Key Points:

- The terrestrial water storage (TWS) over the Tibetan Plateau (TP) decreased faster in the cold season than in the warming season from 1979 to 2019
- Enhanced warming over the TP could cause a transition from snowfall to rainfall by increasing melting level heights
- The slow process associated with decreasing snowfall contributed more to the decreasing TWS recharge than the fast process did during 1979–2019

Supporting Information:

Supporting Information may be found in the online version of this article.

Correspondence to:

Y. He,
heyongli@lzu.edu.cn

Citation:

Wang, G., He, Y., Huang, J., Guan, X., Wang, X., Hu, H., et al. (2022). The influence of precipitation phase changes on the recharge process of terrestrial water storage in the cold season over the Tibetan Plateau. *Journal of Geophysical Research: Atmospheres*, 127, e2021JD035824. <https://doi.org/10.1029/2021JD035824>

Received 7 SEP 2021

Accepted 30 JAN 2022

Author Contributions:

Conceptualization: Yongli He
Funding acquisition: Yongli He
Methodology: Guodong Wang
Project Administration: Yongli He
Software: Guodong Wang, Xiaoxia Wang
Supervision: Yongli He
Validation: Yongli He
Writing – review & editing: Yongli He, Jianping Huang, Xiaodan Guan, Huancui Hu, Shanshan Wang, Yongkun Xie

© 2022. American Geophysical Union.
All Rights Reserved.

The Influence of Precipitation Phase Changes on the Recharge Process of Terrestrial Water Storage in the Cold Season Over the Tibetan Plateau

Guodong Wang¹ , Yongli He^{1,2} , Jianping Huang^{1,2} , Xiaodan Guan^{1,2} , Xiaoxia Wang¹, Huancui Hu³ , Shanshan Wang^{1,2}, and Yongkun Xie² 

¹Key Laboratory for Semi-Arid Climate Change of the Ministry of Education, College of Atmospheric Sciences, Lanzhou University, Lanzhou, China, ²Collaborative Innovation Center for Western Ecological Safety, Lanzhou University, Lanzhou, China, ³Pacific Northwest National Laboratory, Atmospheric Sciences and Global Change Division, Richland, WA, USA

Abstract Climate warming has affected the land surface and atmospheric temperature over the Tibetan Plateau (TP), resulting in a series of hydrological changes, such as atmospheric wetting and decreasing terrestrial water storage (TWS). According to Gravity Recovery and Climate Experiment data, TWS higher than 2,500 m over the TP significantly decreased during the 1979–2019 period, with a more enhanced trend in the cold season. Previous studies have mainly focused on the influence of global warming on the discharge process in the warm season, such as glacier melting, increasing runoff and decreasing snow cover. The changes in atmospheric moisture recharge in the cold season and its contribution to decreasing TWS remain unclear. Based on the time scale, the hydrological process can be divided into slow (snowfall and evaporation) and fast (rainfall and runoff) processes. Our results suggest that the TWS changes in the cold season are dominated by slow processes. Cold-season warming over the TP can increase the atmospheric melting level height (MLH), leading to a transition from snowfall to rainfall. Consequently, the decreasing snowfall and increasing evaporation induced by warming result in a net decrease in atmospheric recharge to the TWS. A quantified contribution of the fast and slow processes to the TWS changes in the cold season indicates that the slow processes play a dominant role over most of the TP, except for the Hexi, Inner, Qaidam, Yangtze, and Yellow Basins. Decreasing atmospheric recharge could accelerate the decrease in TWS, which motivates further investigation to better predict the hydrological response.

1. Introduction

The Tibetan Plateau (TP) is the world's highest plateau with an average elevation of 4,000 m and is referred to as the “Third Pole” of the Earth (Kang et al., 2010; Yao et al., 2012). Due to complex terrain thermal and dynamic effects, the TP significantly alters the regional and global climate, especially via the hydrological cycle (Allen & Ingram, 2002; Xu et al., 2014; Yao et al., 2019). In summer, the TP becomes a massive heating source induced by the heat pump effect and converges the surrounding water vapor toward the plateau (Flohn, 1957; Wu et al., 2012; Xu et al., 2008; Yang et al., 2014; Yao et al., 2015). Moisture over the TP driven by ascending motions can generate abundant precipitation to recharge terrestrial water storage (TWS), which is the water stored in snow cover, glaciers, soil water, groundwater, surface water, and the water contained in animals and plants (Meng et al., 2019; Rodell et al., 2018). Due to the large number of water resources, the TP contains the headwaters of 12 critical rivers in Asia, including the Indus, Ganges, Brahmaputra, Yangtze, and Yellow Rivers. A large amount of water from the TP is transported to the surrounding areas through a vast network of rivers and groundwater aquifers, which provide necessary water resources for humans in the downstream region. Therefore, the TP is also called the “Asian Water Tower” (Lu et al., 2005; Xu et al., 2008).

However, the TP is one of the most sensitive areas to climate change (Bibi et al., 2018; Guan et al., 2015; Huang et al., 2019a, 2019b; Yang et al., 2014). Because of global warming, the TP is experiencing enhanced warming that is twice that of the global mean warming rate during the past four decades, and it is likely to continue in the future (Duan & Xiao, 2015; Rangwala et al., 2009; Zhou & Zhang, 2021). The continued warming trend has led to the acceleration of hydrological cycles. For example, enhanced warming significantly increases surface evaporation and accelerates the precipitation recycling process, which drives increasing atmospheric moisture, that is, the wetting trend (He et al., 2021). On the other hand, the lakes located in the inner TP presented a significant expansion of 32% in the number of lakes and 25% in the lake area during the 1976–2018 period

(Zhang et al., 2019, 2020), which was caused by increased precipitation and glacier melting (Song et al., 2020; Sun et al., 2020). The glaciers in the southeastern part of the TP experienced dramatic mass loss during the 1975–2013 period that was induced by warming and weakening of the Indian monsoon (Liu et al., 2021; Neckel et al., 2014). At the same time, based on simulation results, runoff is increasing due to increasing precipitation and glacier melting (Li et al., 2013; Su et al., 2016). Consequently, the water storage in solid, liquid, and vapor phases over the Asian Water Tower is altered by enhanced warming, which transforms solid water (glaciers and snow cover) to liquid water (runoff and lakes) and can impact the supply of the Asian Water Tower. Recent studies have found that the overall TWS is decreasing dramatically due to increased runoff and glacier melting, although an increasing trend in the inner TP is due to lake expansion (Liu et al., 2021; Meng et al., 2019).

According to the seasonal cycle of the TWS on the TP that peaks in August and minimizes in December, we can generally divide the TWS dynamics into two phases: the recharge phase from the atmosphere to the TWS due to a net increase in precipitation minus evaporation in the cold season (October to April) and the discharge phase in the warm season (May to September), which dominates runoff. While most of the earlier attention has been given to the direct impact of surface warming in the warm season, which leads to glacier melting, increasing evaporation, and runoff, the indirect impact of surface warming in the cold season when the TWS recharges through changes in the atmospheric circulation and structure remains unclear. Multiple recent studies indicate that such an indirect impact of surface warming in the cold season can be important. Tropospheric temperature and humidity directly impact the composition of clouds, the microphysical process of cloud formation, and the dynamics of clouds and ultimately influence the subsequent precipitation (Pruppacher & Klett, 2012). A recent study (Prein & Heymsfield, 2020) found that the melting level height (MLH) increased by 32 m/decade over global land areas during the 1979–2010 period, which could cause a transition from snowfall to rainfall. Consistently, recent studies found that over the TP, snowfall decreases, although the total precipitation and rainfall increase (Deng et al., 2017; Wang et al., 2016).

The snowfall/rainfall ratio changes induced by the precipitation phase transition can be important for the atmospheric recharge process. Precipitation minus evaporation usually indicates the atmospheric recharge ability to TWS. However, snowfall and rainfall have different residence times in the components of TWS. Over the TP, a large amount of snowfall continuously accumulates in the solid form during the cold season and can be stored long term, therefore indicating a slow process to the TWS. In contrast, rainfall would rapidly run off or can be further delayed by infiltrating into the soils, which is likely to have a faster transit in the TWS system and indicates a faster hydrologic process in the terrestrial system. Given their different time scales of impact on the TWS and the fact that most of the TWS on the TP is stored in the solid form, such as snow cover, glaciers, and soil moisture, snowfall and rainfall may have a different impact on the atmospheric recharge ability to the TWS. This question becomes more important because the snowfall/rainfall ratio in precipitation is likely changing in response to the enhanced warming over the TP and how precipitation phase changes can affect the recharging of the TWS would have critical implications for the water resource changes of the Asian Water Tower under enhanced warming.

This study aims to understand the response of atmospheric recharge processes (mainly through precipitation) to enhanced warming over the TP and its contributions to the decreasing TWS in recent decades (1979–2019). There are two key questions we want to address: (a) how important are the atmospheric recharge processes via precipitation to the TWS changes under enhanced warming over the TP? (b) What is the mechanism for the changes in the atmospheric recharge processes, and how does it contribute to the decreasing TWS? Answers to these questions are critical for understanding the hydrological response over the TP to global warming and its projection.

The rest of this study is arranged as follows. Section 2 describes the data and methodology used in this study, including the MLH calculation and water budget analysis. Section 3 examines the changes in the recharge and discharge processes of the Asian Water Tower, the influence of precipitation type changes on the recharge, and its quantified contribution. Section 4 discusses the linkage between those processes and presents a summary of this study.

2. Data and Methodology

2.1. Satellite and Reanalysis Data Sets

The Gravity Recovery and Climate Experiment (GRACE) is a new method to monitor global water resources and retrieve changes in terrestrial water storage. It consists of a binary star system launched in March 2002 and was jointly developed by the National Aeronautics and Space Administration (NASA) and the German Aerospace Center (DLR, or Deutsches Zentrum für Luft-und Raumfahrt). It uses a precision-ranging system mounted on the satellite to measure the distance changes between the satellites and uses a new calculation scheme to invert the global gravity field changes. Mass concentration blocks (mascons) are new solutions that use prior constraints in space and time to estimate the gravity field to minimize measurement errors and are currently available (Watkins et al., 2015). GRACE satellite data are mainly processed, released, and managed by the Jet Propulsion Laboratory (JPL) of NASA, the Center for Space Research (CSR) of the University of Texas, and the German Research Center for Geosciences (GFZ, or GeoForschungZentrum). Our research uses CSR RL06 Mascon Solutions (version 01) data (Save et al., 2016) with a resolution of 0.25° (April 2002–June 2017) and Goddard Space Flight Center (GSFC) RL06 Mascon Solutions (version 02.4) data (Loomis et al., 2019) with a resolution of 0.5° (January 2003–July 2016).

Due to the lack of long-term observation data over the TP, reanalysis data are an effective alternative to investigate this region's climate changes. The latest state-of-the-art reanalysis data set provided by the European Center for Medium-Range Weather Forecasts (ECMWF) is the fifth-generation reanalysis global atmosphere (ERA5) data set, which improves the data assimilation process and the simulation of physical processes (Hersbach et al., 2020). Many previous studies have applied ERA5 data to study climate changes over the TP (He et al., 2021; Xu et al., 2020). The ERA5 data set correlates with GRACE satellite data and has been used to investigate the atmospheric-terrestrial water cycle over the TP (Lei et al., 2021). To analyze the recharge ability of TWS and explain its changes in recent decades, we used the monthly surface temperature, total column water (TCW), total precipitation, snowfall, evaporation, and runoff from the ERA5 reanalysis data set. The rainfall was calculated by total precipitation minus snowfall. The resolution is 0.25° × 0.25° horizontally, with 37 levels in the vertical direction. The data set covers the period from January 1979 to December 2020 (Hersbach et al., 2020). The climatology was calculated using the mean values from 1979 to 2020. Due to the high elevation and cold climate over the TP, the warm season (May to September) is very short, and the cold season (October to April) is relatively long. To reduce the uncertainty, the changes in the above hydrological components from ERA5 were compared with those in the Japanese 55-year Reanalysis (JRA-55) and High Asia Refined analysis version 2 (HARv2) data sets. JRA55 uses the offline simple biosphere model forced with precipitation corrected by the Special Sensor Microwave/Imager (SSM/I) brightness temperature and assimilates a few stations over the eastern Tibetan Plateau from 1971 to 2006 (Kobayashi et al., 2015; Onogi et al., 2005). HARv2 was generated by dynamical downscaling of global ERA5 using the Weather Research and Forecasting (WRF) model (X. Wang et al., 2021).

2.2. Dynamic Threshold Parameterization Scheme

Before investigating the changes in snowfall over the TP, the quality of snowfall in the ERA5 data set should be validated. Here, we use the estimated snowfall determined by the dynamic threshold parameterization scheme (DTPS), which is an empirical method to distinguish precipitation types through surface air conditions (Ding et al., 2014). Through comparison with station observations, this method has been demonstrated to capture snowfall changes over the TP successfully (Ding et al., 2014). The precipitation type is decided by

$$type = \begin{cases} snow, & T_w \leq T_{min} \\ sleet, & T_{min} < T_w < T_{max} \\ rain, & T_w \geq T_{max} \end{cases} \quad (1)$$

where T_w is the wet-bulb temperature, which is more useful than the dry-bulb temperature because it considers evaporative cooling effects (Bocchieri, 1980). The two threshold temperatures (T_{min} and T_{max}) are given below:

$$T_{min} = \begin{cases} T_0 - \Delta S \times \ln \left[\exp \left(\frac{\Delta T}{\Delta S} \right) - 2 \times \exp \left(-\frac{\Delta T}{\Delta S} \right) \right], & \frac{\Delta T}{\Delta S} > \ln 2 \\ T_0 & , \frac{\Delta T}{\Delta S} \leq \ln 2 \end{cases} \quad (2)$$

$$T_{max} = \begin{cases} 2 \times T_0 - T_{min}, & \frac{\Delta T}{\Delta S} > \ln 2 \\ T_0 & , \frac{\Delta T}{\Delta S} \leq \ln 2 \end{cases} \quad (3)$$

The three parameters (ΔS , ΔT , and T_0) in Equations 2 and 3 are obtained by elevation (Z) and ERA5 hourly relative humidity (RH) data from Equations 4–6.

$$\Delta S = 2.374 - 1.634 \times RH \quad (4)$$

$$\Delta T = 0.215 - 0.099 \times RH + 1.018 \times RH^2 \quad (5)$$

$$T_0 = -5.87 - 0.1042 \times Z + 0.0885 \times Z^2 + 16.06 \times RH - 9.614 \times RH^2 \quad (6)$$

For the meaning and derivation details of the above items, the reader should refer to Ding et al. (2014). Notably, the DTPS considers the physical process of snowfall melting and focuses on elevation and surface meteorological data to retain the two threshold temperatures on each grid dynamic. Therefore, the DTPS is an accurate and effective method to distinguish precipitation types over the TP, and it has been used in many studies (Deng et al., 2017; Luo et al., 2020; Yang et al., 2021; Zhu et al., 2017).

2.3. Melting Level Height

The MLH has a strong influence on the precipitation type because the ice particles will not begin melting until the ambient wet-bulb temperature (or ice bulb temperature) reaches 0°C (Prein & Heymsfield, 2020; Wilson, 1941). The MLH is defined as the vertical height of the zero-degree wet-bulb temperature above the surface. The higher the MLH is, the more negligible the probability of snowfall and the greater the probability of rainfall. Therefore, understanding the response of the MLH to enhanced warming is the key to investigating the mechanism of precipitation phase changes.

The wet-bulb temperature was calculated using air temperature and specific humidity (Prein & Heymsfield, 2020). It is considerably difficult to obtain the exact melting level (ML) geopotential directly from the pressure level data due to the low vertical resolution. The model-level data in the ERA5 data set have 137 model levels in the vertical direction, which is better for accurately calculating the geopotential height of zero-degree wet-bulb temperature by interpolation. However, the geopotential height is provided at the surface but not at the model level in ERA5. Therefore, hourly reanalysis output for ERA5 model levels was used to calculate the wet-bulb temperature T_w . To represent the vertical direction of the dependent variables, temperature, and specific humidity, the atmosphere is divided into layers according to the total number of model levels (NLEV). The model half-level pressure is given by

$$P_{k+1/2} = a_{k+1/2} + b_{k+1/2} \cdot sp \quad (7)$$

where $P_{k+1/2}$ denotes the pressure at the half level ($k + 1/2$ level) with $0 \leq k \leq \text{NLEV}$, sp is the surface pressure, and $a_{k+1/2}$ and $b_{k+1/2}$ are coefficients that define the model levels. The pressure at a full model level k is given by the average of the pressure between the two bounding half levels:

$$P_k = \frac{P_{k-1/2} + P_{k+1/2}}{2} \quad (8)$$

where P_k denotes the pressure at the full level (k level), with $1 \leq k \leq \text{NLEV}$, $k + 1/2$ is the half level below the full model level k and $k - 1/2$ is the half level above. $P_{k-1/2}$ and $P_{k+1/2}$ refer to the pressures at the model half levels above and below, respectively. Moreover, the key parameter T_w (unit: °C) at a full model level k can be deduced (Ding et al., 2014) as

$$(T_w)_k = T_k - \frac{e_{sat}(T_k) \times (1 - RH_k)}{0.000643 \times P_k + \frac{\partial e_{sat}(T_k)}{\partial T_k}} \quad (9)$$

$$e_{sat}(T_k) = 6.1078 \times \exp\left(\frac{17.27 \times T_k}{T_k + 273.3}\right) \quad (10)$$

The above parameters of $(T_w)_k$, T_k and RH_k in Equations 9 and 10 represent the wet-bulb temperature, air temperature and relative humidity at the full level (k level); $e_{sat}(T_k)$ is the saturated vapor pressure at T_k by Tetens's empirical formula (Murray, 1967).

Moreover, the full-level geopotential height is calculated by the following method of vertical integration:

$$\phi_{k+\frac{1}{2}} = \phi_s + \sum_{j=k+1}^{NLEV} R_d \cdot (T_v)_j \cdot \ln\left(\frac{P_{j+\frac{1}{2}}}{P_{j-\frac{1}{2}}}\right) \quad (11)$$

$$\phi_k = \phi_{k+\frac{1}{2}} + \alpha_k \cdot R_d \cdot (T_v)_k \quad (12)$$

where ϕ_s is the geopotential height of the Earth's surface and $\phi_{k+1/2}$ is the geopotential height at the $k+1/2$ half level. The gas constant for dry air is represented by R_d , while the virtual temperature is represented by T_v , and α_k is defined as

$$\alpha_k = \begin{cases} \ln 2, & k = 1 \\ 1 - \frac{P_{k-\frac{1}{2}}}{P_{k-\frac{1}{2}} - P_{k-\frac{1}{2}}} \cdot \ln\left(\frac{P_{k-\frac{1}{2}}}{P_{k-\frac{1}{2}}}\right), & k > 1 \end{cases} \quad (13)$$

Simmons and Burridge (1981) discussed in detail the physical reasons for this vertical discretization scheme. The geopotential height of the zero wet-bulb temperature level is estimated by linearly interpolating between the two closest models' full-level geopotentials that enclose the ML. Finally, the geopotential height of the ML is transformed into the MLH above the surface. The values of a and b coefficients in Equation (7) and half-level- and full-level pressure are all obtained from the ECMWF website (<https://www.ecmwf.int/en/forecasts/documentation-and-support/137-model-levels>).

2.4. Analysis of the Water Budget

Based on the land surface water balance (Lei et al., 2021; Meng et al., 2019), the changes in TWS are associated with precipitation (including snowfall and rainfall), evaporation, and runoff, as shown below:

$$\text{TWSC} = \text{Snowfall} + \text{Rainfall} - E - R + \text{Res} \quad (14)$$

The changes in TWS (TWSC) include soil moisture, snow water equivalent, glaciers, rivers and groundwater. E represents evaporation, R represents runoff, and Res represents the residual term. The nonclosure of the land surface water balance is mainly induced by the data assimilation methods in the reanalysis data set (He et al., 2021; Meng et al., 2019). As noted before, we separate snowfall and rainfall into slow and fast processes, respectively, according to their time scales of impact on the TWS. For a similar reason, we now divide evaporation and runoff into slow and fast processes that mainly explain the loss of the TWS.

The GRACE TWS estimates are anomalies of the total land water mass relative to the mean values throughout 2004–2010. The TWS anomalies within the TP were spatially integrated to obtain the monthly time series of TWS over the TP. The TWSC was defined as the difference between two successive GRACE monthly anomalies:

$$\text{TWSC}_i = \text{TWS}_{i+1} - \text{TWS}_i \quad (15)$$

where TWS_i and TWS_{i+1} are the GRACE monthly anomalies of month i and month $i+1$, respectively. We obtain the simulated TWS in each month as shown in the following equation:

$$TWS_{i+1} = TWS_i + TWSC_i = TWS_i + \text{Snowfall}_i + \text{Rainfall}_i - E_i - R_i \quad (16)$$

By integrating the right term in Equation (16) based on the ERA5 data set, we obtained the accumulated changes in TWS during each cold season, which is usually positive and indicates that the TWS recharges during the cold season. Then, we compared the contributions of snowfall, rainfall, evaporation and runoff to the trends of cold season-accumulated TWSC.

3. Results

3.1. Changes in the Recharge and Discharge of the Asian Water Tower

Because of global warming, the near-surface air temperature of the TP has risen, and the annual average surface temperature has increased at a rate of $0.332^{\circ}\text{C}/\text{decade}$ with a 99% confidence level during the 1979–2020 period (Figure 1a), which is consistent with a previous study (Duan & Xiao, 2015; Rangwala et al., 2009; Zhou & Zhang, 2021). The northeastern, central, and western parts of the TP had apparent warming trends; the maximum value of the warming trend in the northeastern part of the TP exceeded $0.55^{\circ}\text{C}/\text{decade}$ during the 1979–2020 period (Figure 1c). During the same period, the TCW increased by $0.118 \text{ kg/m}^2/\text{decade}$ from 1979 to 2020 (Figure 1a), which means that the atmosphere over the TP became wetter. However, the terrestrial water storage anomaly (TWSA) changes in the CSR and GSFC data sets from GRACE consistently showed a decreasing trend, with rates of -9.05 Gt/year and -8.22 Gt/year during the 2002–2017 period, respectively (Figure 1b). However, an opposite trend occurred with an increase in the northern TP and a decrease in the southern TP (Figures 1e and 1f). The decreasing TWSA was mainly distributed in the Himalayas and Brahmaputra Valley. The increasing trend in the TWSA in the CSR and GSFC data sets occurred in the northern TP, extending more westward in the GSFC data set (Figures 1e and 1f).

To investigate the variation in the TWSA over the TP, Figure 2 shows the time series of the monthly, cold season- and warm season-averaged TWSA over the TP from 2002 to 2017 based on the CSR and GSFC data sets. There was a seasonal cycle in the TWSA, with a maximum in July/August and a minimum in December to February (Figures 2a and 10a). For the long-term period, a significant decreasing trend was observed in the CSR and GSFC data sets, with -9.55 Gt/year during the 2002–2017 period and -8.24 Gt/year during the 2003–2016 period. From the perspective of the hydrological cycle, the TWS should discharge mainly in the warm season through runoff and then recharge in the cold season through snowfall. To investigate the reason for the enhanced decrease in the TWSA, we examined the TWSA trends in the cold season and warm season (Figures 2c and 2e). The results suggest that the TWSA in the cold season decreased at rates of -9.91 Gt/year and -9.64 Gt/year , which are more significant than those in the warm season over the TP (-7.99 Gt/year and -7.06 Gt/year). The TWSC represents the net recharge of TWS in the cold season and the net discharge of TWS in the warm season. Figure 2 investigates the variation in the TWSC in the annual, cold season and warm season. The TWSC in the cold season decreased faster than that in the warm season, although their trend did not pass the significance test. Therefore, the mechanism of decreasing TWS in the cold season deserves more investigation. Many studies have investigated the changes in TWS from the perspective of land surface water balance and found that the variation in precipitation played a dominant role in the TWS accumulation upstream of the Yangtze and Yellow Basins (Meng et al., 2019). This suggests that we should examine precipitation changes in the cold season.

3.2. Influence of Precipitation Type Changes on the Recharge Process

3.2.1. Evaluation of Snowfall in ERA5 Over the TP

Previous study found that the snowfall may have a large bias in ERA5 data set due to the overestimation of precipitation climatology (Bian et al., 2019). Therefore, before investigating the precipitation type changes, the quality of snowfall in the ERA5 data set should be evaluated to decrease the uncertainty of the following analysis. Due to the lack of observations in the western TP, the DTPS method was considered to capture snowfall and rainfall successfully (Ding et al., 2014) and is used to distinguish precipitation types over the TP based on the hourly ERA5 data set. Figure 3 compares the snowfall from the ERA5 and DTPS methods during the 1979–2020

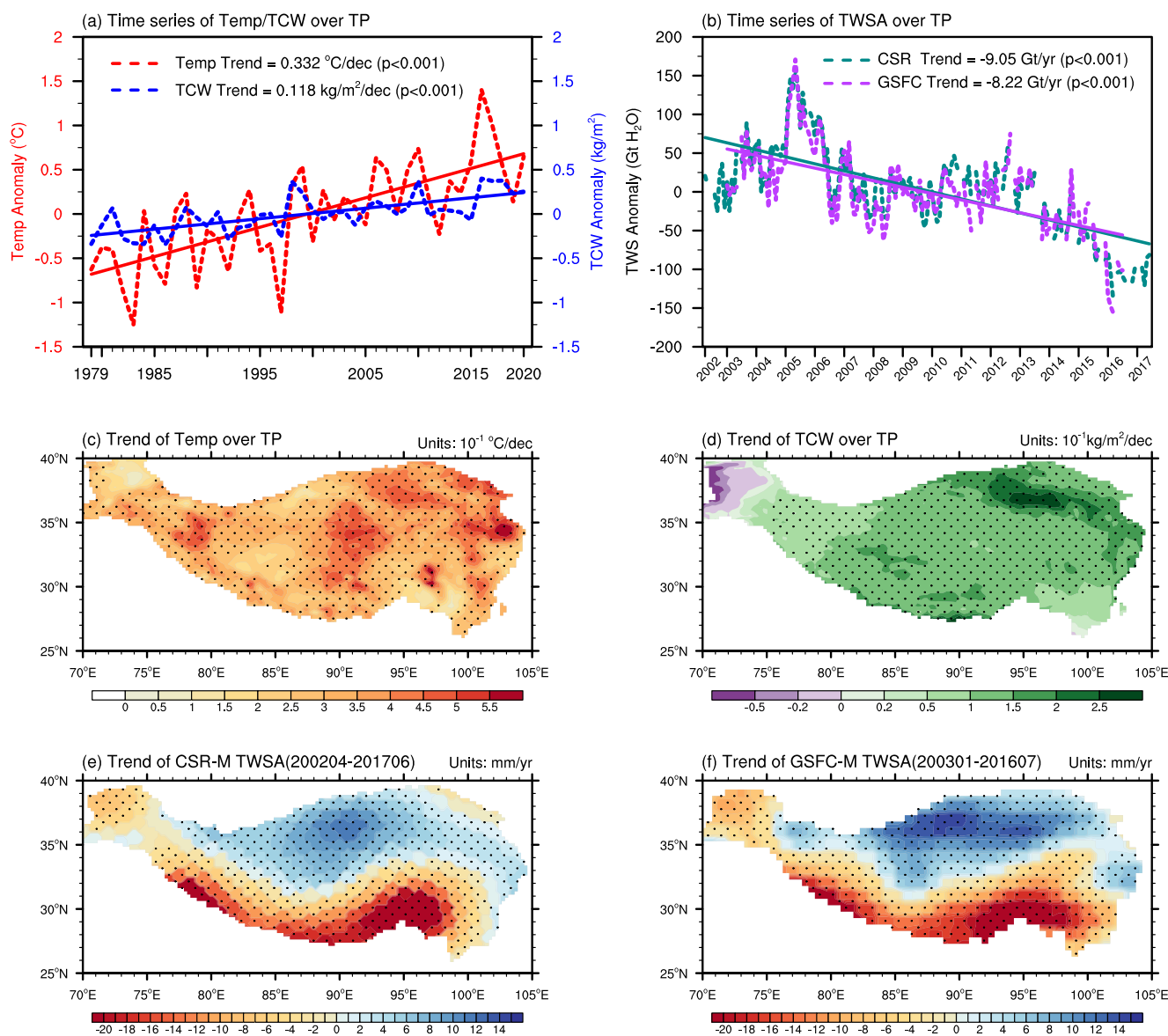


Figure 1. (a) Time series of the surface air temperature (red line) and TCW (blue line) over the Tibetan Plateau (TP) during the 1979–2020 period. (b) The time series of the TWSA from the Center for Space Research (CSR) (green line) and GSFC (purple line) data sets over the TP during the 2002–2017 period. The trend map of the surface air temperature (c) and TCW (d) over the TP during the 1979–2020 period; the counter area indicates the extent of the TP, where the elevation is higher than 2,500 m. The trend of the TWSA from the CSR (e) and GSFC (f) over the TP during the 2002–2017 period. The dotted areas indicate statistical significance exceeding 95%.

period. The result suggests a high correlation (0.979) between the monthly snowfall from ERA5 and the DTSPS method. In the annual variation, the annual snowfall from ERA5 and the DTSPS method is also consistent, and the correlation coefficient reaches 0.986, with a 99% significance level. Although ERA5 overestimates snowfall over the TP relative to the DTSPS, the root mean square error (RMSE) between the monthly snowfall in ERA5 and the DTSPS is small enough (3.115 mm) not to affect the analysis of precipitation type changes. The above results show that the snowfall over the TP from ERA5 and the DTSPS methods is similar on monthly, annual, and interdecadal scales. Therefore, the snowfall from ERA5 can capture the characteristics of long-term trends and could be used to analyze precipitation type changes.

To reduce the uncertainty, the changes in the above hydrological components from ERA5 were compared with those in the JRA-55 and HARv2 data sets (Figure S1 and Table S1 in Supporting Information S1). The correlation coefficients of total precipitation, snowfall, rainfall and snowfall-to-rainfall ratio between ERA5 and

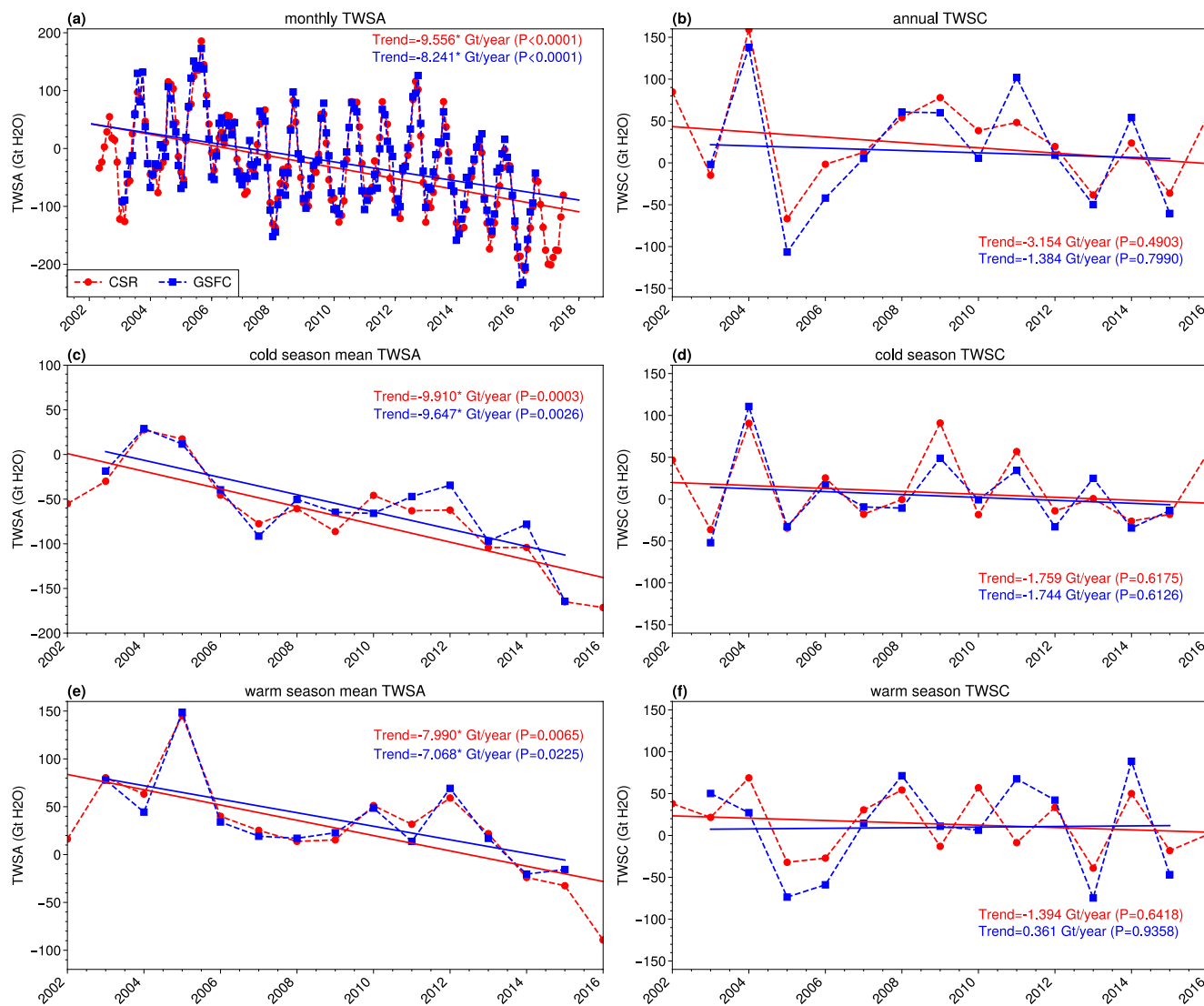


Figure 2. (a) Time series of the (a) annual, (b) cold season, and (c) warm season mean TWSA (left column) and cumulative TWSC (right column) from the Center for Space Research and GSFC data sets over the 2002–2017 period.

JRA-55/HARv2 reach 0.822/0.883, 0.904/0.937, 0.648/0.739, and 0.877/0.933, respectively, with a 99% confidence level. Runoff and evaporation behave less than precipitation, but their trends remained consistent with ERA5. These results show a consistent variation in hydrological components between the three data sets.

3.2.2. Precipitation Type Changes

Atmospheric recharge to surface water storage is determined by the amount of precipitation minus evaporation and is also related to the precipitation types. Snowfall could directly replenish the glacier and snow cover and accumulate the TWSA in the cold season to offset the discharge by runoff in the warm season. To investigate the changes in atmospheric recharge, we first investigated the changes in the precipitation type. Figures 4a–4c shows the monthly climatology and trends of total precipitation, rainfall, and snowfall over the TP. Consistent with previous studies, the climatology of total precipitation was dominated by rainfall in the warm season. The climatology of snowfall is relatively less than that of rainfall, with two maximum values in March and October. Due to the increasing TCW and accelerated precipitation recycling associated with warming in summer, the total precipitation and rainfall both exhibited significant increasing trends in the warm season (Figures 4a and 4b). The rainfall in the cold season did not exhibit a significant trend, and the total precipitation even exhibited a decreasing trend (Figure 4d). As shown in Figure 4c, snowfall exhibited a decreasing trend during most of the months,

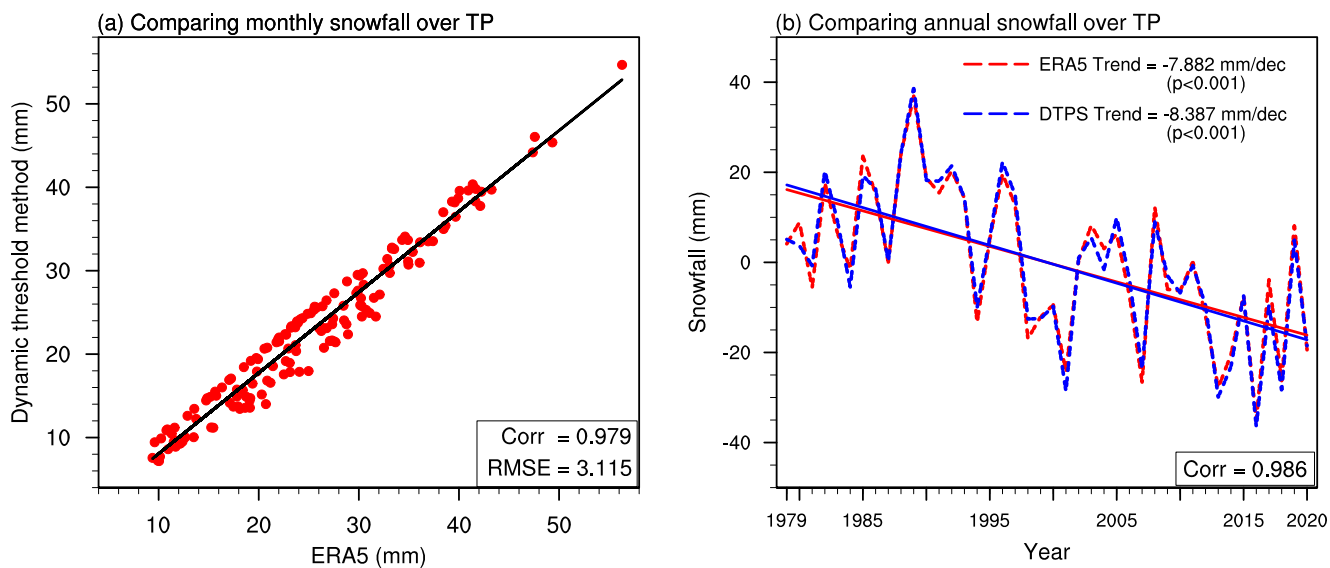


Figure 3. (a) Comparison between the monthly snowfall based on the ERA5 data set and simulated values from the dynamic threshold parameterization scheme (DTPS) over the Tibetan Plateau (TP) during the 1979–2020 period. (b) Time series of annual snowfall anomalies over the TP from the ERA5 data set and DTPS method. The Pearson correlation coefficient exceeds the 99% confidence level.

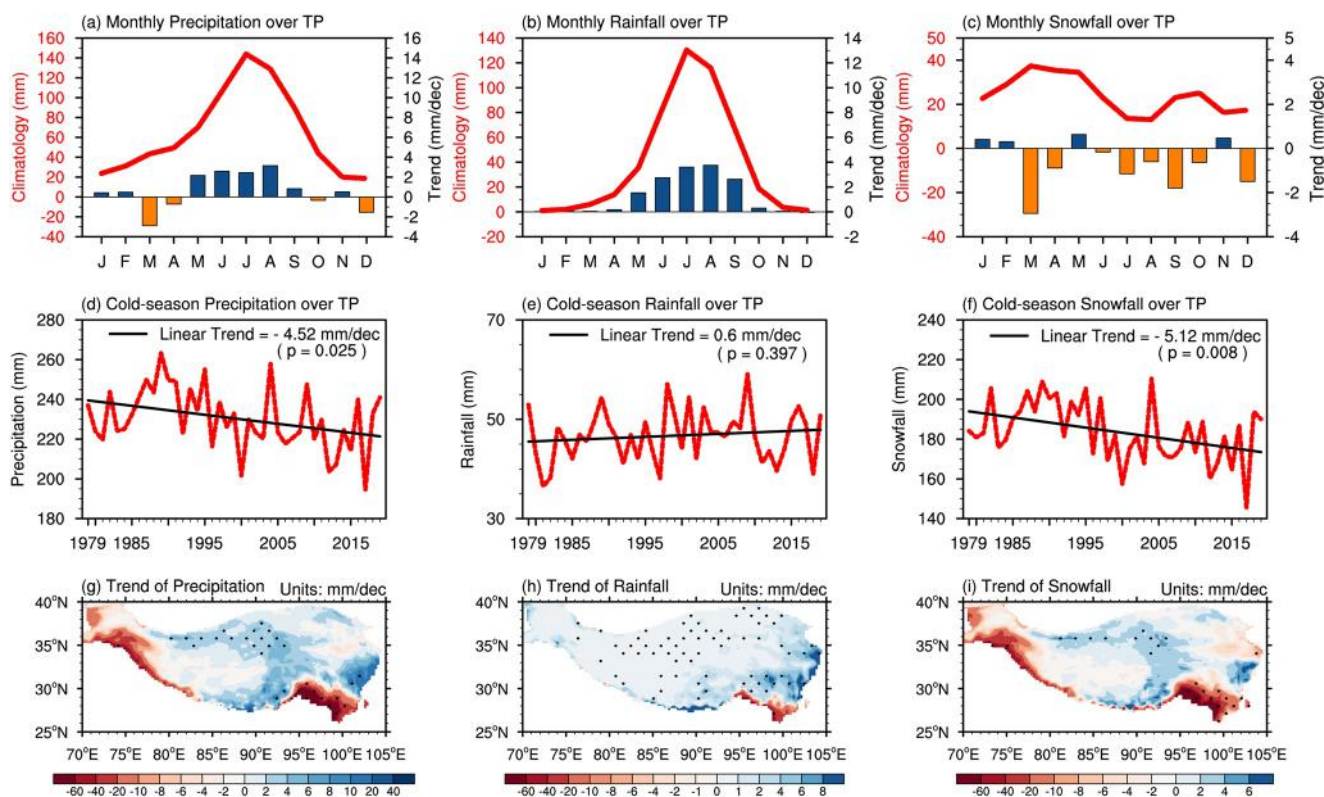


Figure 4. (a) Monthly climatology (lines) and trends (bars) of annual precipitation, (b) rainfall, (c) and snowfall over the Tibetan Plateau (TP) during the 1979–2020 period. (d) Time series of cumulative precipitation, (e) rainfall, (f) and snowfall in the cold season over the TP. (g) Trends of precipitation, (h) rainfall, (i) and snowfall in the cold season over the TP during the 1979–2019 period. The dotted areas indicate statistical significance exceeding 95%.

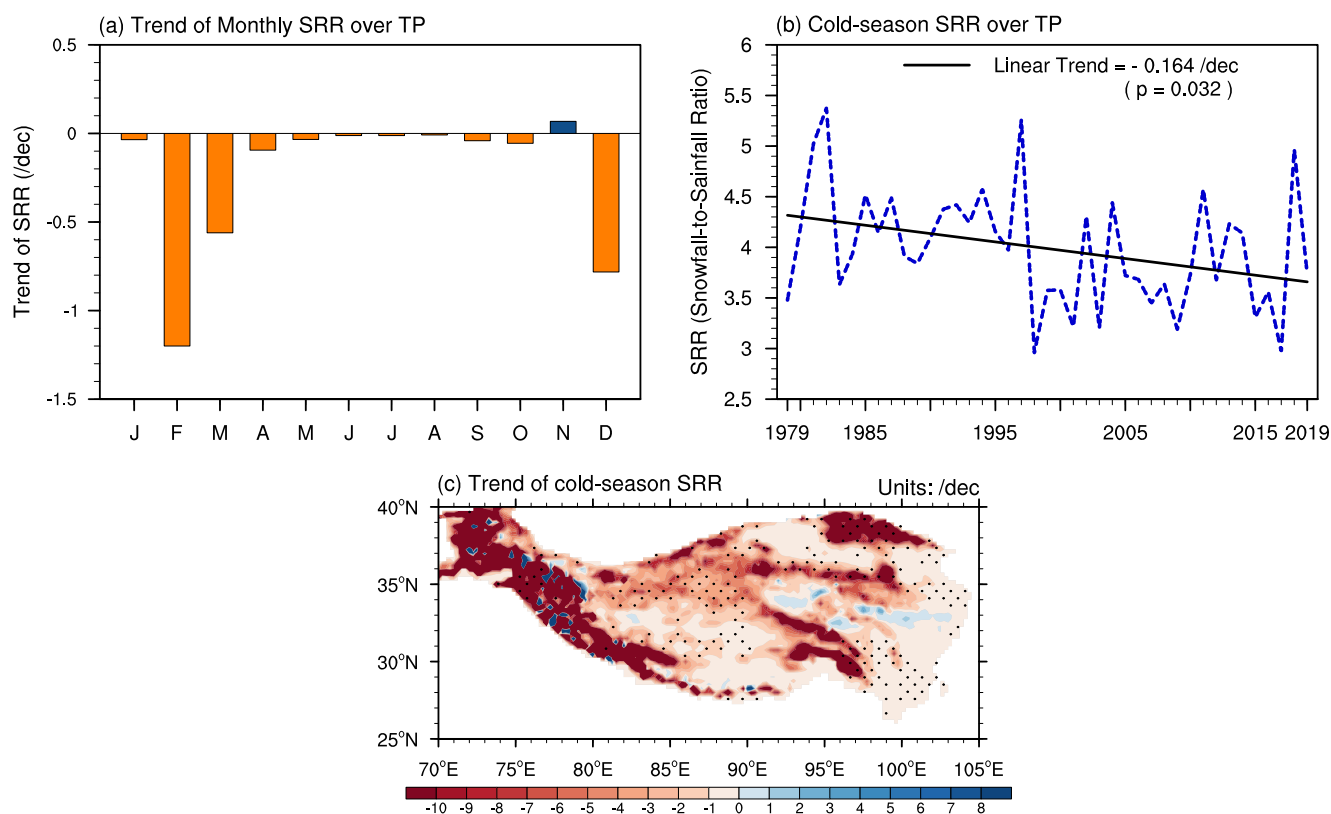


Figure 5. (a) Monthly trends of the regionally averaged snowfall-to-rainfall ratio (SRR) over the Tibetan Plateau (TP) during the 1979–2020 period. (b) Time series of the averaged SRR in the cold season over the TP during the 1979–2019 period. (c) Trend distribution of the SRR in the cold season over the TP during the 1979–2019 period. The dotted areas indicate statistical significance exceeding 95%.

especially in March, September, and December, which suggests that the snowfall response to enhanced warming is different from that of rainfall.

To further investigate the changes in rainfall and snowfall during the cold season, Figures 4e and 4f shows the time series of rainfall and snowfall during the cold season from 1979 to 2020. The result suggests that the rainfall in the cold season is increasing with a weak trend of 0.6 mm/decade and that the snowfall in the cold season is decreasing with a significant trend of -5.12 mm/decade . However, the distribution of the total precipitation and snowfall trends in the cold season was highly spatially variable (Figures 4g and 4i). The total precipitation trend significantly decreased in the southwestern and southeastern TP, which was mainly caused by the decreasing snowfall there. The central and northern TP both experienced increasing rainfall and snowfall. The trend in rainfall during the cold season generally increased, except for the southeastern TP (Figure 4h). The enhanced cold season warming supports the increased rainfall by increasing the TCW. However, it may also support some of the snowfall melting and conversion into rainfall, resulting in an increase in rainfall during the cold season.

The ratio of snowfall to rainfall has gradually received increasing attention from the scientific community in recent years (Deng et al., 2017; Prein & Heymsfield, 2020; Wang et al., 2016). The larger the snowfall-to-rainfall ratio (SRR) is, the more snowfall there is relative to rainfall. Figure 5a shows that the SRR decreases throughout the year except for November and is most significant during the cold season, especially in February. The averaged SRR over the TP in the cold season shows a decreasing trend, with a rate of $-0.164 / \text{decade}$ (Figure 5b). Spatially, the SRR in the cold season decreases over most of the TP, especially in the southwest and central areas. However, sporadic areas show an increasing trend, which may be caused by the small denominator.

3.2.3. Changes in Atmospheric Recharge Associated With Precipitation Type Changes

Precipitation and evaporation are the main methods of water exchange between the atmosphere and the terrestrial surface and represent the net amount of water received by the surface, which plays a vital role in the land

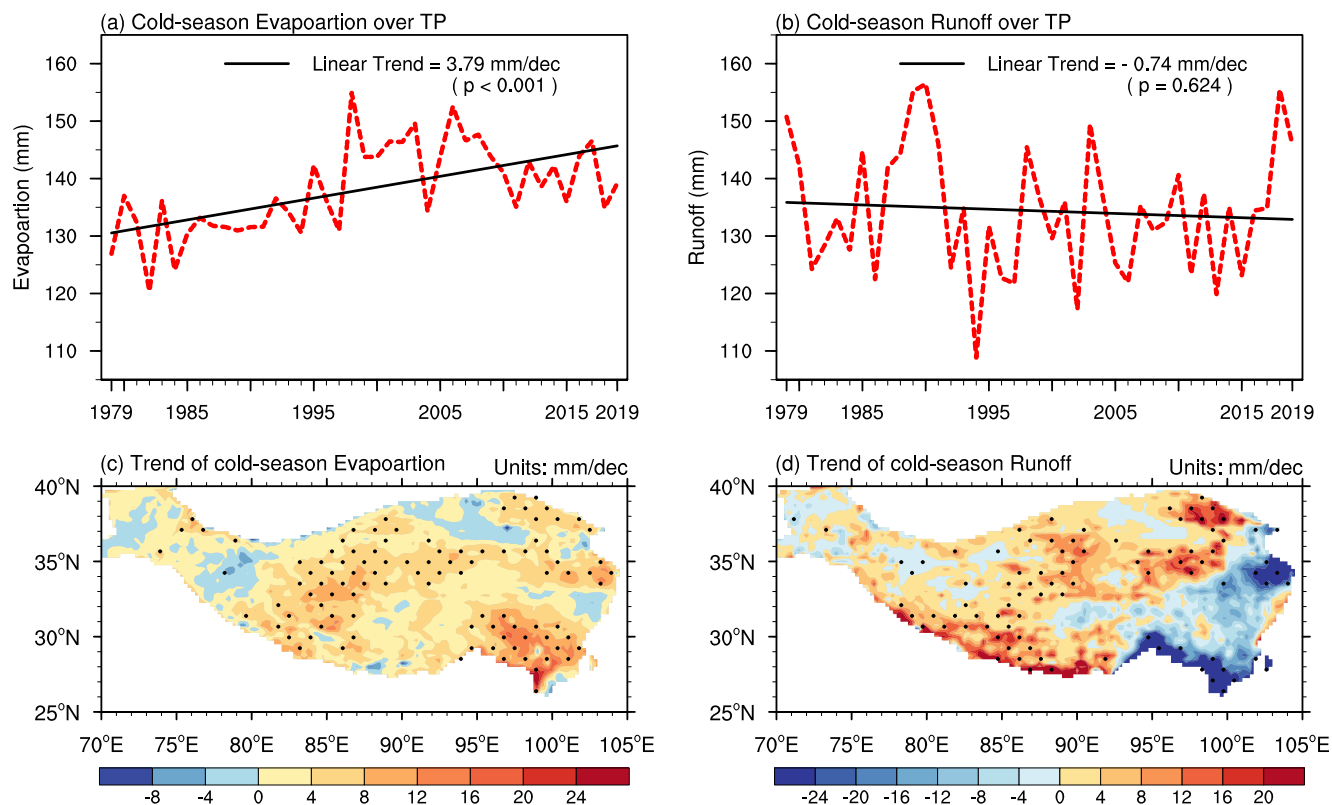


Figure 6. Time series of evaporation (a) and runoff (b) in the cold season over the Tibetan Plateau (TP) during the 1979–2019 period. Trends of evaporation (c) and runoff (d) in the cold season over the TP during the 1979–2019 period. The dotted areas indicate statistical significance exceeding 95%.

surface water balance. Therefore, previous studies have used precipitation minus evaporation (P-E) to represent the atmospheric recharge ability of the land surface and discovered a “dry becomes drier and wet becomes wetter” pattern in global dry/wet changes (Byrne & O’Gorman, 2015; Liu & Allan, 2013). Over the TP, glacier melting, as the primary discharge process, is attributed to the leading cause of decreasing TWS. Few studies note the changes in the atmospheric recharge process associated with precipitation and evaporation. However, atmospheric recharge characterized by precipitation minus evaporation does not consider the effect of changes in the precipitation phase. Precipitation can be divided into rainfall and snowfall according to its type. It should be pointed out that recharge by rainfall is a fast process. When rainfall reaches the ground, some of the rain stays on the surface or penetrates into the ground, while the rest is rapidly lost through runoff and evaporation, especially for heavy rainfall, which has a more significant proportion of loss. On the other hand, the recharge of snowfall to the TWS is a slow process. Snowfall usually remains in the solid form for a few months until it melts and then slowly penetrates into the ground in the warm season.

According to the land surface water balance, evaporation and runoff, as the discharge process, could also impact the changes in TWS. As surface warming occurs during the cold season over the TP, evaporation increases in most areas of the TP, especially in the southeastern TP (Figures 6a and 6c). Although there was a slightly decreasing trend in the average runoff in the cold season over the TP during the 1979–2019 period, the runoff significantly increased in the central and western TP, which is one possible reason for the TWS decrease there (Figures 6b and 6d).

Due to the covariance between precipitation, evaporation and runoff, partial correlation analysis was used. Table 1 compares the partial correlation coefficients between the TWS changes and each component of the land-surface water balance equation, including snowfall, rainfall, evaporation and runoff in the warm and cold seasons. The partial correlation coefficient between the TWSC and the amount of snowfall reaches 0.796/0.916 in the cold season based on the CSR and GSFC data sets, respectively, which is higher than that in the warm season (0.645/0.491). The results suggest that snowfall has a larger partial correlation coefficient than other terms in

Table 1

Partial Correlation Coefficients Between Snowfall, Rainfall, Evaporation, Runoff, Snowfall-Evaporation, Rainfall-Runoff and TWSA Based on the CSR and GSFC Data Sets Over the TP

Correlation coefficient		Snowfall	Rainfall	Evaporation	Runoff	Snowfall-evaporation	Rainfall-runoff
TWSA in the cold season	CSR	0.796 ^a	0.293	-0.315	-0.56 ^c	0.806 ^a	0.578 ^b
	GSFC	0.916 ^a	-0.115	-0.38	-0.75 ^b	0.842 ^a	0.435
TWSA in the warm season	CSR	0.645 ^a	0.504 ^c	-0.277	0.10 ^c	0.687 ^a	0.539 ^c
	GSFC	0.491	0.071	-0.094	0.24	0.587 ^a	0.141

^aSignificant confidence levels of 99%. ^bSignificant confidence levels of 95%. ^cSignificant confidence levels of 90%.

both the cold season and warm season. The rainfall is much greater than snowfall in the warm season; however, it would flow out of the Tibetan Plateau soon through increasing runoff. Therefore, the changes in TWS need to be investigated from the perspective of fast and slow processes. “Snowfall-Evaporation” represents the net water flux in the slow processes of the hydrological cycle, and “Rainfall-Runoff” represents the net water flux in the fast process of the hydrological cycle. The partial correlation coefficients between the TWSC and fast/slow process were also calculated as shown in Table 1. The results demonstrate that slow processes have a much higher correlation (0.806/0.842) with the TWSC than fast processes (0.578/0.435) in the cold season. This result suggests that slow processes in the cold season have a more critical impact on the TWS changes. However, the partial correlation coefficients between the slow process and TWSC would decrease in the warm season, which may be associated with more rainfall and runoff in the warm season than in the cold season. Therefore, slow processes associated with snowfall-evaporation indicate the effective recharge ability of the atmosphere to TWS in the cold season.

Figure 7a shows the monthly climatology of the effective recharge ability (snowfall-evaporation). It is positive from October to April, representing recharge, and it is negative from May to September, representing discharge. For the long-term trend, the effective recharge ability significantly decreases throughout the year except for a weak increasing trend in November, January, and February (Figure 7a). Focusing on the cold season, the results suggest that the average effective recharge ability has a significant decreasing trend at a rate of -7.67 mm/decade (Figure 7b). The most significant decreasing trend was concentrated in the southwestern and southeastern TP (Figure 7c), which is similar to the spatial trend of the TWSA (Figures 1e and 1f), indicating that the effective recharge ability has a close relationship with the TWSC.

3.3. Mechanism of the Influences of Significant Warming on the Recharge Process

3.3.1. Influence of the Melting Level Height on the Precipitation Type Changes

Figure 8a shows the monthly trend of the MLH over the TP. The result suggests that the MLH increased throughout the year, with the most significant trend in November (Figure 8a). The average MLH over the TP in the cold season increased by 6.26 m/year (Figure 8b), which is twice that of the global land average value. Compared with the surface temperature in the cold season, the correlation coefficient between the MLH and surface temperature reaches 0.946 and passes the significance test at the 99% confidence level, which indicates that the increasing MLH has been mainly dominated by surface warming (Figure 8b). The spatial distribution of the MLH trend during the 1979–2019 period shows that the MLH exhibited the most significant increasing trends in the southern TP, where snowfall significantly decreased (Figure 8c). The correlation coefficients between the MLH and snowfall over the southern TP could exceed -0.8 at the 99% confidence level (Figure 8d), suggesting an essential impact of the MLH on snowfall changes. However, there is a positive correlation between the MLH and snowfall in the northwestern TP, which suggests that other mechanisms also influence snowfall variability, such as the increasing atmospheric moisture in the cold season. As the MLH increased in the cold season during the 1979–2019 period, the amount of snowfall decreased and transformed into rainfall, which is consistent with the results in Figure 4.

To verify the effect of the MLH on the precipitation phase during the cold season over the TP, the relationship between the MLH and rainfall and snowfall during the past 40 years was examined, as shown in Figure 9. The correlation coefficients between the cold season-averaged MLH and snowfall and rainfall are 0.536 and -0.533,

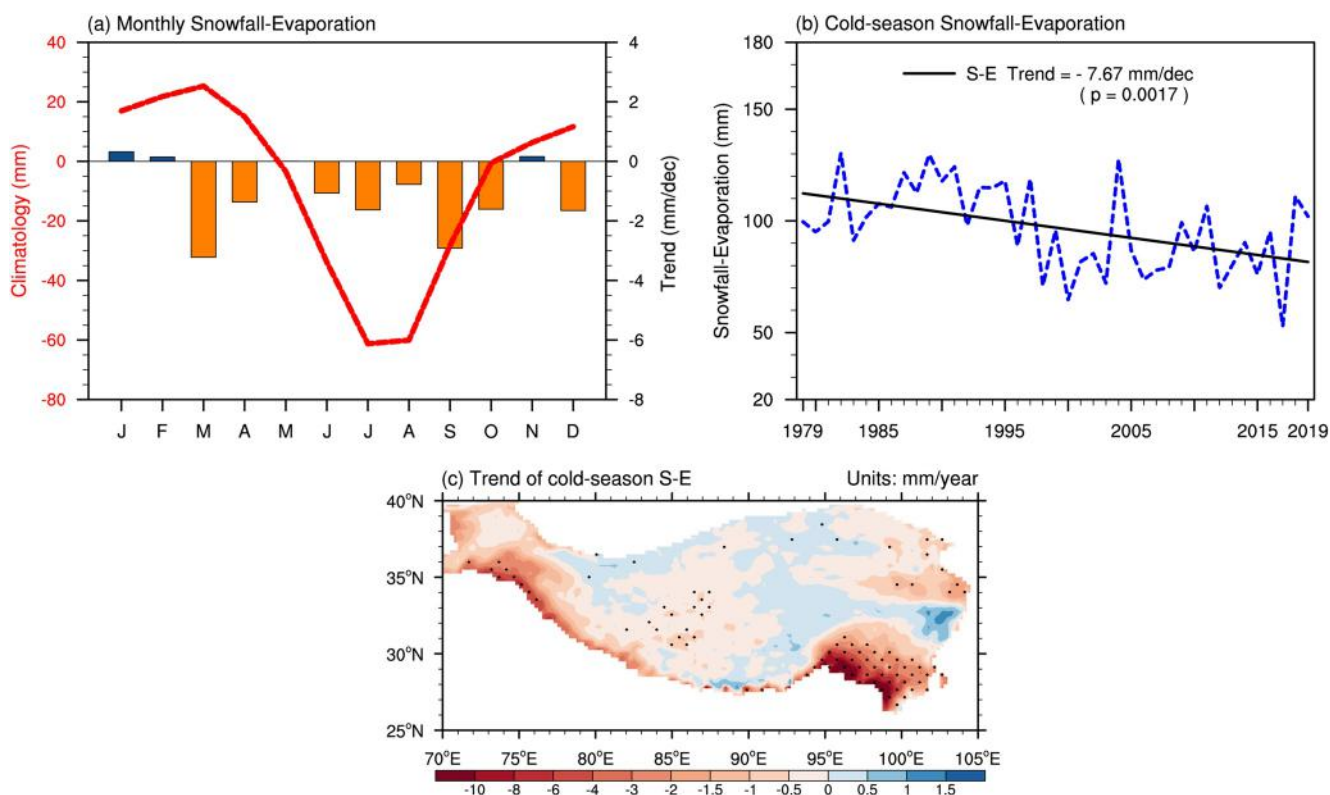


Figure 7. (a) Monthly climatology (lines) and trends (bars) of regionally averaged snowfall-evaporation over the Tibetan Plateau (TP) during the 1979–2019 period. (b) Time series of snowfall-evaporation in the cold season over the TP during the 1979–2019 period. (c) Trend distribution of snowfall-evaporation in the cold season over the TP during the 1979–2019 period. The dotted areas indicate statistical significance exceeding 95%.

respectively. The linear regression results showed that for every 1 m increase in the MLH, the average rainfall during the cold season over the TP increased by 0.034 mm, and the snowfall decreased by 0.061 mm (Figure 9). Therefore, the increase in the MLH induced by enhanced warming in the cold season would decrease the ratio of snowfall to rainfall and further impact the atmospheric recharge process.

3.3.2. Quantification of the Recharge Process Contribution to the Decreasing TWS

Given the changes in different terms in the water budget, we now examine the contribution of the fast and slow processes of the hydrological cycle. Due to the limitation of the length of GRACE observations, it is difficult to investigate the response of fast and slow processes and their contribution to the decreasing TWS for a long period. However, a recent study demonstrated that the simulated TWS from the water budget equation based on the ERA5 data set contains a consistent variation in TWS with GRACE observations (Lei et al., 2021). Therefore, this consistent variation provides an opportunity to investigate the long-term trend of fast and slow processes based on the ERA5 data set. First, we need to assess the consistency between the observed TWSA in the GRACE data set and the estimated TWSA from the water balance equation based on the reanalysis data set. Figure 10a shows the monthly mean values and trend of the observed TWSA from the CSR and GSFC data sets and the estimated TWSA calculated from the water balance equation in the cold season during the 2003–2015 period. The results demonstrated that the estimated TWSA could capture the annual cycle of the observed TWSA, with the correlation coefficient between the monthly simulated and observed TWSA ranging from 0.6 to 0.8 (Figure 10a). Figure 10b compares the interannual variation in the estimated and observed cold season mean TWSC and shows that the correlation coefficient between the observed and estimated cold season mean TWSC reached 0.698 and 0.702 with 99% confidence levels, respectively. Therefore, we can use the water balance terms to investigate the variation in the TWSC over the TP in the cold season.

Due to the contrasting trends of GRACE in the southern and northern TP, as shown in Figure 1, it is necessary to investigate the contribution of fast and slow processes to the TWSC variations specifically in each basin over

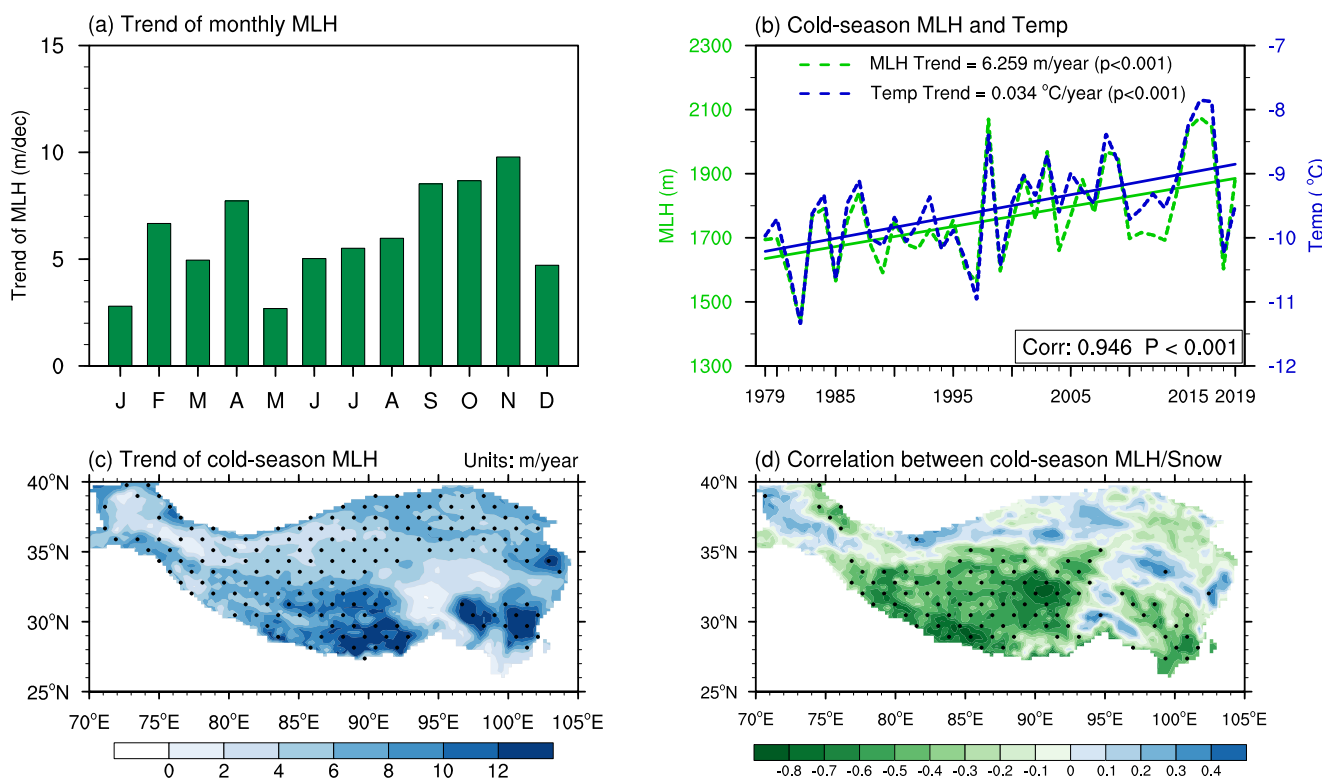


Figure 8. (a) Monthly trends of the averaged melting level height (MLH) over the Tibetan Plateau (TP) during the 1979–2020 period. (b) Time series of the surface air temperature and MLH in the cold season over the TP during the 1979–2019 period. (c) Trend distribution of the MLH in the cold season over the TP during the 1979–2019 period. (d) Correlation map between the MLH and snowfall in the cold season over the TP during the 1979–2019 period. The dotted areas indicate statistical significance exceeding 95%.

the TP as shown in Figure 11. When integrating the water budget equation in a one-month period, the left term in Equation (14) becomes the TWSC, and the right term in Equation (14) becomes the monthly accumulated variables. A negative TWSC indicates a decreasing trend of TWS, and a positive TWSC indicates an increasing trend of TWS. To be consistent with the observed TWSA from the GRACE data set, the anomaly of the estimated TWSC from the ERA5 data set is calculated relative to the same period of 2004–2010. Table 2 shows the mean values of the anomaly of estimated TWSC and the anomalies of snowfall, rainfall, evaporation, and runoff during the 2002–2017 period.

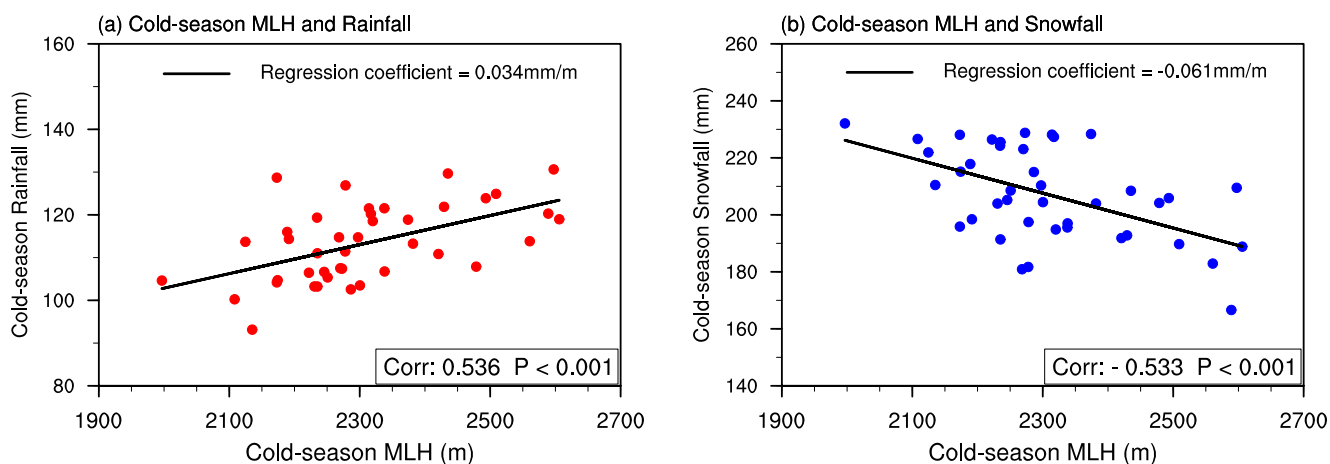


Figure 9. Scatter distribution of rainfall (a) and snowfall (b) with the melting level height in the cold season over the Tibetan Plateau and their regression relationship.

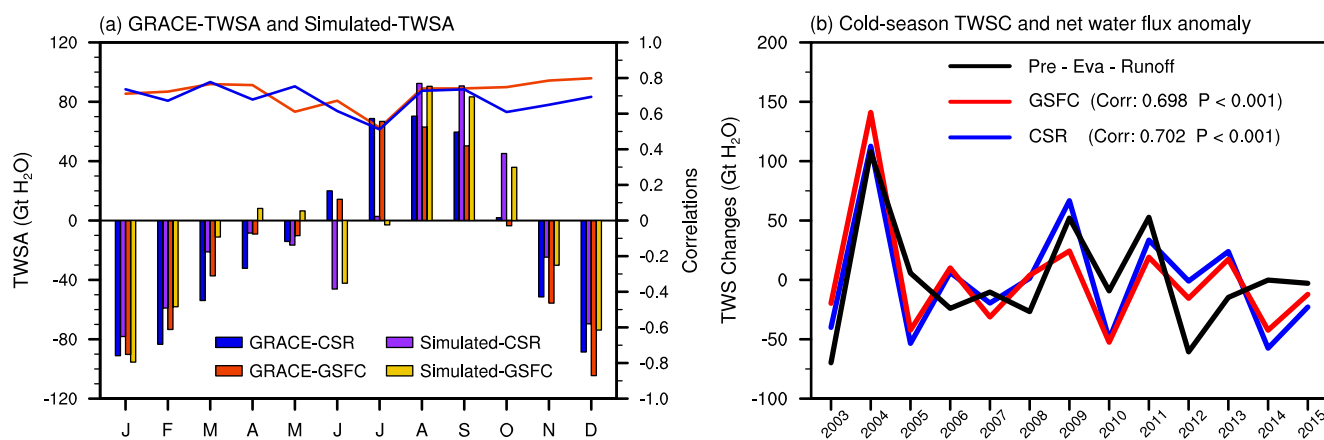


Figure 10. (a) Monthly mean Gravity Recovery and Climate Experiment (GRACE)-observed TWSA (blue/red bars represent Center for Space Research (CSR)/GSFC data; units, Gt) and ERA5-simulated TWSA by integrating the net water flux (purple/yellow bars represent simulated values based on the initial CSR/GSFC data; units, Gt) over the Tibetan Plateau (TP) during the 2003–2015 period. Temporal correlations between the observed TWSA and estimated TWSA are calculated each month and shown as solid lines (blue/red lines represent CSR/GSFC data, respectively). (b) GRACE-observed TWSC anomalies in the cold season compared with the ERA5-estimated TWSC anomaly (integration of the precipitation-evaporation-runoff (pre-eva-runoff) anomaly in the cold season) over the TP during the 2002–2015 period.

Based on Figure 11, the southern TP mainly includes the Brahmaputra Basin, and the northern TP mainly includes the Inner and Qaidam Basins. The TWSC anomaly in the Brahmaputra Basin was negative, and the TWSC anomalies in the Inner and Qaidam Basins were positive, which is consistent with Figures 1e and 1f. For the Brahmaputra Basin, snowfall and rainfall anomalies are both negative, which is associated with decreasing water vapor transportation from the Indian Ocean. At the same time, the runoff anomaly is also negative, which may be related to decreasing precipitation, although it may be increased by glacier melting. The contributions of rainfall and runoff are opposite and offset to the TWSC; therefore, the result suggests that slow processes contribute

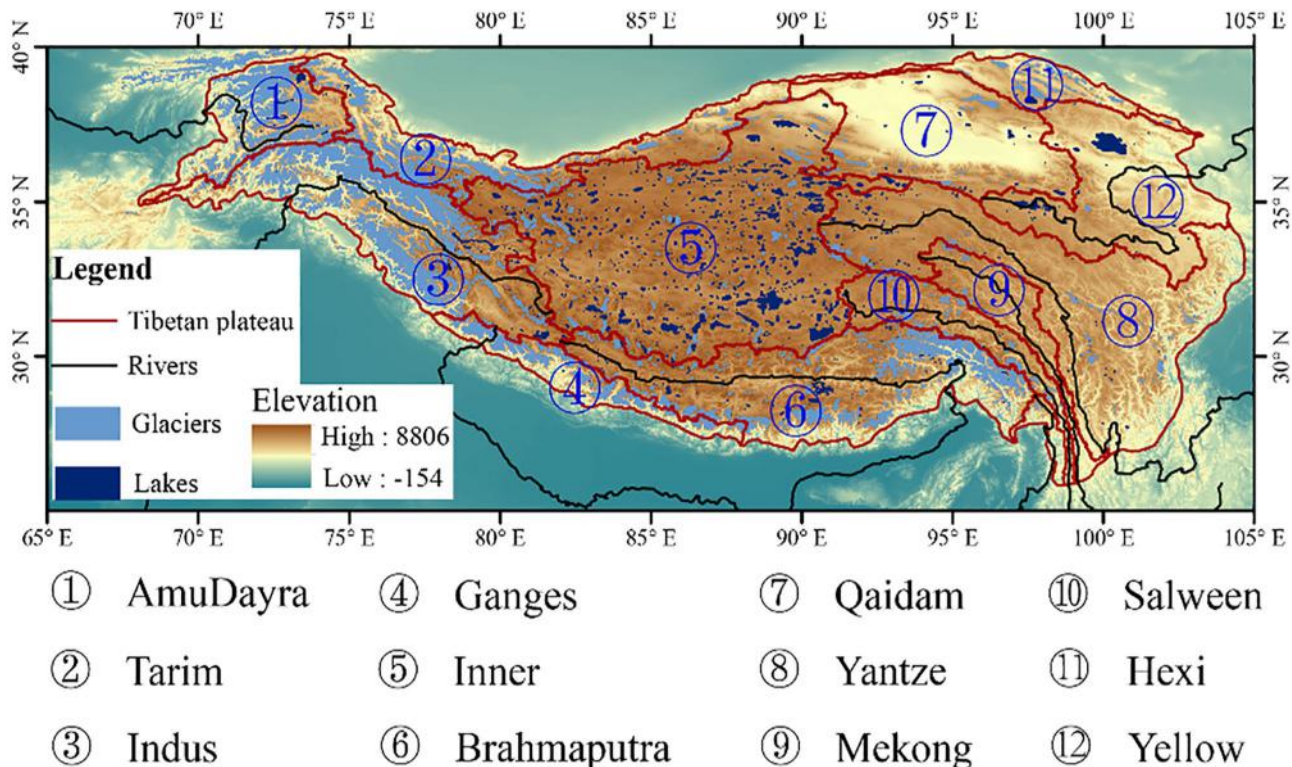


Figure 11. Geographic location of the 12 basins on the Tibetan Plateau.

Table 2

Mean Anomalies of the Estimated TWSC, Terms in the Water Balance Equation (Snowfall, Rainfall, Evaporation, and Runoff), and Fast and Slow Processes in the Cold Season Over the Entire TP and 12 Subbasins During the 2002–2017 Period

Basins	Simulated TWSC	Snowfall	Rainfall	Evaporation	Runoff	Snowfall - evaporation	Rainfall-runoff
Total TP	−18.2445	−18.0003 (98.66%)	−8.3208 (45.61%)	−0.2413 (−1.32%)	−7.8354 (−42.95%)	−17.7590 (97.34%)	−0.4855 (2.66%)
AmuDayra	1.1103	1.0231 (92.14%)	0.0516 (4.65%)	0.1602 (−14.43%)	−0.1958 (17.64%)	0.8629 (77.71%)	0.2474 (22.29%)
Brahmaputra	−5.7053	−4.6519 (81.54%)	−5.3644 (94.02%)	0.2110 (3.7%)	−4.5219 (−79.26%)	−4.8628 (85.23%)	−0.8425 (14.77%)
Ganges	1.2600	0.2124 (16.86%)	0.8462 (67.16%)	−0.1456 (11.56%)	−0.0557 (4.42%)	0.3581 (28.42%)	0.9019 (71.58%)
Hexi	−0.0437	−0.0378 (−86.51%)	−0.0195 (44.62%)	0.0018 (4.14%)	0.0602 (137.75%)	−0.0360 (−82.37%)	−0.0797 (182.37%)
Indus	−4.9402	−5.3200 (107.69%)	0.3765 (−7.62%)	0.0136 (0.27%)	−0.0168 (−0.34%)	−5.3335 (107.96%)	0.3933 (−7.96%)
Inner	0.6423	−0.9543 (−148.56%)	−0.2222 (−34.59%)	−1.2994 (202.29%)	−0.5194 (80.86%)	0.3451 (53.73%)	0.2972 (46.27%)
Mekong	−1.2109	−1.1984 (98.97%)	−0.2816 (23.26%)	0.5494 (45.37%)	−0.8185 (−67.60%)	−1.7478 (144.34%)	0.5369 (−44.34%)
Qaidam	0.2703	−0.0958 (−35.45%)	−0.0168 (−6.22%)	−0.5012 (185.42%)	0.1183 (−43.76%)	0.4054 (149.98%)	−0.1351 (−49.98%)
Salween	−2.3717	−1.9696 (83.04%)	−0.4861 (20.49%)	0.4456 (18.79%)	−0.5295 (−22.33%)	−2.4152 (101.83%)	0.0435 (−1.83%)
Tarim	−0.4839	−0.1376 (28.42%)	0.0579 (−11.96%)	0.5190 (107.25%)	−0.1148 (−23.72%)	−0.6566 (135.67%)	0.1726 (−35.67%)
Yangtze	−4.1203	−3.3601 (82%)	−1.3236 (32%)	0.5392 (13%)	−1.1026 (−27%)	−3.8993 (95%)	−0.2211 (5%)
Yellow	−1.6035	−0.7413 (46%)	−0.5865 (37%)	−0.8213 (−51%)	1.0970 (68%)	0.0799 (−5%)	−1.6834 (105%)

Note. Units; Gt. The anomalies are relative to the climatology during the 2004–2010 period. Numbers in the brackets indicate the contributions (%) of each term to the mean TWSC.

more to the negative TWSC anomaly than fast processes. For the Inner and Qaidam Basins, the negative anomaly of snowfall is less than that of rainfall, which suggests that snowfall decreases faster than rainfall. In contrast to the Brahmaputra Basin, the evaporation anomaly is much lower and contributes more to the TWSC anomaly. Therefore, the slow process plays a more important role in the TWSC anomalies than the fast process, especially for the Qaidam Basin.

In the cold season, the recharge process is usually stronger than the discharge process; therefore, the TWSC in the cold season indicates the net recharge ability of the TWS. To further investigate the trend of the net recharge ability of TWS, Table 3 shows the trends of the estimated TWSC, the terms of the water budget equation in the cold season over each basin, and the whole TP during the 1979–2019 period. The trends of estimated cold-season TWSC over the whole TP and each basin are all negative, as shown in Table 3, suggesting that the recharge ability of TWS in each basin decreases in the cold season, with the most significant decrease in the Brahmaputra and Indus Basins. A further comparison of the contributions of the fast and slow processes to the trends of the recharge ability revealed that the slow processes associated with snowfall and evaporation had a dominant contribution to the whole TP, except for the Hexi, Inner, Qaidam, Yangtze, and Yellow Basins. Note that over the Yangtze and Yellow Basins, the trends of the simulated TWSC are much smaller and nearly zero due to the opposite contribution of the fast and slow processes. Considering the relative contributions of snowfall and evaporation changes to the recharge process separately, the contribution of snowfall is higher than that of evaporation over these basins, where slow processes dominate the recharge ability trends, except for the Tarim Basin. Therefore, the result supports that the decreasing recharge ability over the TP in the cold season is determined by slow processes, especially by changes in snowfall.

4. Discussion

4.1. Response of Atmospheric Recharge to Enhanced Warming in the Cold Season and Its Mechanism

The following provides a physical picture of how the precipitation phase changes influence the atmospheric recharge process and contribute to the decreasing TWS over the TP. The mechanism causing the changes in the effective atmospheric recharge is summarized as a schematic diagram (Figure 12). Previous studies have demonstrated that climate warming over the TP has induced glacier-accelerated melting and expansion of lakes, which could increase runoff and evaporation. However, climate warming over the TP could affect the atmospheric

Table 3

Trends of the Estimated TWSC, Terms in the Water Balance Equation (Snowfall, Rainfall, Evaporation, and Runoff), and Fast and Slow Processes in the Cold Season Over the Entire TP and 12 Subbasins During the 1979–2019 Period

Basins	Simulated-TWSC	Snowfall	Rainfall	Evaporation	Runoff	Snowfall - evaporation	Rainfall-runoff
Total TP	−2.1132	−1.6958 (80.25%)	−0.1043 (4.93%)	0.8402 (39.76%)	−0.5270 (−24.94%)	−2.5360 (120.01%)	0.4228 (−20.01%)
AmuDayra	−0.0882	−0.0836 (90.48%)	0.0065 (−7.42%)	0.0116 (13.13%)	−0.0005 (−0.52%)	−0.0952 (107.93%)	0.0070 (−7.93%)
Brahmaputra	−0.5561	−0.5004 (89.99%)	−0.1993 (35.84%)	0.1394 (25.08%)	−0.2831 (−50.91%)	−0.6399 (115.07%)	0.0838 (−15.07%)
Ganges	−0.1629	−0.1007 (61.81%)	0.0520 (−31.89%)	0.0446 (27.38%)	0.0696 (42.7%)	−0.1453 (89.19%)	−0.0176 (10.81%)
Hexi	−0.0483	0.0082 (−17.07%)	0.0050 (−10.36%)	0.0204 (42.25%)	0.0411 (85.19%)	−0.0121 (25.18%)	−0.0361 (74.82%)
Indus	−0.6292	−0.5331 (84.72%)	0.0145 (−2.3%)	0.0688 (10.93%)	0.0418 (6.65%)	−0.6019 (95.65%)	−0.0274 (4.35%)
Inner	−0.2138	0.0428 (−20%)	0.0349 (−16.33%)	0.1587 (74.22%)	0.1328 (62.11%)	−0.1159 (54.22%)	−0.0979 (45.78%)
Mekong	−0.0650	−0.0719 (110.63%)	−0.0149 (22.92%)	0.0413 (63.48%)	−0.0631 (−97.02%)	−0.1132 (174.1%)	0.0482 (−74.1%)
Qaidam	−0.0391	0.0151 (−38.57%)	0.0140 (−35.68%)	0.0173 (44.27%)	0.0509 (129.98%)	−0.0022 (5.71%)	−0.0369 (94.29%)
Salween	−0.1285	−0.1474 (114.71%)	−0.0217 (16.89%)	0.0544 (42.33%)	−0.0950 (−73.94%)	−0.2017 (157.04%)	0.0733 (−57.04%)
Tarim	−0.0522	−0.0094 (18.05%)	0.0076 (−14.64%)	0.0286 (54.76%)	0.0218 (41.84%)	−0.0380 (72.8%)	−0.0142 (27.2%)
Yangtze	−0.0074	−0.1372 (1,860%)	0.0998 (−1,354%)	0.1497 (2,030%)	−0.1797 (−2,436%)	−0.2869 (3,890%)	0.2795 (−3,790%)
Yellow	0.0007	−0.0586 (−7,906%)	0.0599 (8,073%)	0.0786 (−10,608%)	−0.0782 (10,541%)	−0.1373 (−18,514%)	0.1380 (18,614%)

Note. Units; Gt/yr. Numbers in the brackets indicate the contributions (%) of each term to the TWSC trend.

structure and indirectly affect the balance between recharge and discharge processes. Consistent with a previous study (Prein & Heymsfield, 2020), enhanced warming in the cold season has a good correlation with increasing MLH, which is a crucial parameter to determine the ratio of rainfall to snowfall. When the MLH increases due to warming, the atmospheric structure favors the transition from snowfall to rainfall. From the land-surface water balance equation, we can divide them into fast processes (rainfall and runoff) and slow processes (snowfall and evaporation). A comparison of the assessment of the fast and slow process changes and their contribution to the TWSC reveals that the slow processes play a dominant role in the variation in TWS, especially in the cold season. However, climate warming can directly increase evaporation and indirectly decrease snowfall by increasing the MLH, thereby reducing the atmospheric recharge ability and then TWS. However, the contribution of the fast and slow processes has considerable uncertainty due to the reanalysis data set's quality, such as the overestimated precipitation associated with a low-resolution representation of the complex topography. Therefore, additional work will be required to investigate this mechanism.

4.2. Implications of the Changes in Atmospheric Recharge Under Warming

Glaciers, snow cover, and other solid forms of water are an essential part of the Asian Water Tower. The amount of solid water determines the sustainability of the Asian Water Tower. Previous studies have noted that climate warming threatens glaciers and snow cover, which are decreasing dramatically. Researchers have hoped that increased precipitation induced by atmospheric wetting would help glaciers and snow cover recover. However, the indirect effect of climate warming through increasing the MLH would partly offset the increase in snowfall induced by atmospheric wetting. The near-term and long-term projections of climate over the TP show continued warming and wetting trends, suggesting that the atmospheric recharge ability will continue to decrease and affect the balance between recharge and discharge. Therefore, investigations of hydrological changes in the future should pay more attention to the changes in the atmospheric recharge process, especially for snowfall.

5. Conclusion

Because the TWS over the TP can only be recharged through precipitation, the changes in the atmospheric recharge processes under climate warming are crucial to the variation in TWS. Although the TCW in the atmosphere over the TP is increasing, the TWS shows a significant decreasing trend. While previous studies mostly focused on the role of increasing runoff on the decreasing TWS, we examined the changes in the atmospheric

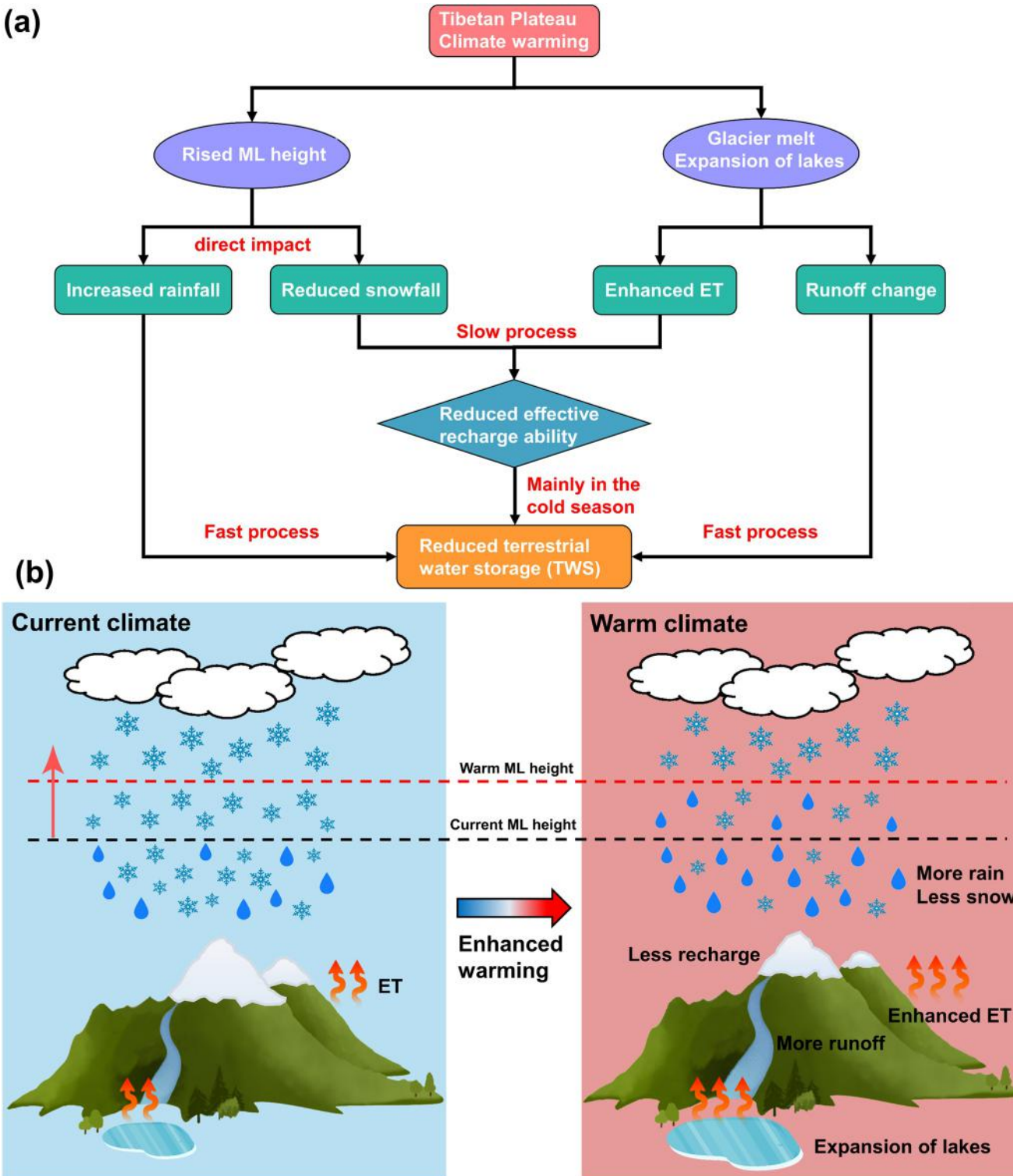


Figure 12. Schematic illustration of the physical process of terrestrial water storage reduction induced by warming over the Tibetan Plateau.

recharge processes in response to climate warming and the contributions to the decreasing TWS in this study. Based on the GRACE data set, we found that the decrease in TWS in the cold season was faster than that in the warm season. The terms in the water budget equation are further divided into fast (rainfall and runoff) and slow (snowfall and evaporation) processes on various time scales. The slow processes indicate a more effective role in

the atmospheric recharge ability and thus dominate the variations in the TWS, which mainly occurs in the cold season. However, the effectiveness of this slow process in recharging the TWS is decreasing. Further investigation suggests that the enhanced warming in the cold season could increase the MLH, which induces the transition from snowfall to rainfall. Decreasing snowfall and increasing evaporation induced by climate warming therefore significantly decrease the atmospheric recharge ability to the TWS. According to the consistent variations of the estimated and observed TWS, we quantify the contribution of the fast and slow processes to the trend of accumulated TWS changes in the cold season for recent decades (1979–2019). The results suggest that slow processes play a dominant role in accumulated TWS changes in the cold season on most of the TP, except for the Hexi, Inner, Qaidam, Yangtze, and Yellow Basins. The decreasing atmospheric recharge ability induced by climate warming remains highly uncertain due to the quality of the reanalysis data set and deserves more investigation in the future.

Data Availability Statement

The ERA5 data are available at <https://cds.climate.copernicus.eu>.

Acknowledgments

This work was jointly supported by the Strategic Priority Research Program of the Chinese Academy of Sciences (XDA2006010301), the National Science Foundation of China (42041004, 41521004, 41705047 and 91837209), the National Key Research and Development Program of China (No. 2019YFA0607104), the China 111 Project (B13045) and the Fundamental Research Funds for the Central Universities (Izujbky-2021-sp07). This work was also supported by the Supercomputing Center of Lanzhou University. HH is supported by the U.S. Department of Energy Office of Science Biological and Environmental Research as part of the Regional and Global Modeling and Analysis program area. Pacific Northwest National Laboratory (PNNL) is operated for the Department of Energy by Battelle Memorial Institute under contract DE-AC05-76RL01830.

References

Allen, M. R., & Ingram, W. J. (2002). Constraints on future changes in climate and the hydrologic cycle. *Nature*, 419(6903), 228–232. <https://doi.org/10.1038/nature01092>

Bian, Q., Xu, Z., Zhao, L., Zhang, Y.-F., Zheng, H., Shi, C., et al. (2019). Evaluation and intercomparison of multiple snow water equivalent products over the Tibetan Plateau. *Journal of Hydrometeorology*, 20(10), 2043–2055. <https://doi.org/10.1175/JHM-D-19-0011.1>

Bibi, S., Wang, L., Li, X., Zhou, J., Chen, D., & Yao, T. (2018). Climatic and associated cryospheric, biospheric, and hydrological changes on the Tibetan Plateau: A review. *International Journal of Climatology*, 38, e1–e17. <https://doi.org/10.1002/joc.5411>

Boccchieri, J. R. (1980). The objective use of upper air soundings to specify precipitation type. *Monthly Weather Review*, 108(5), 5962–6003. [https://doi.org/10.1175/1520-0493\(1980\)108<5962:tuouua>2.0.co;2](https://doi.org/10.1175/1520-0493(1980)108<5962:tuouua>2.0.co;2)

Byrne, M. P., & O'Gorman, P. A. (2015). The response of precipitation minus evapotranspiration to climate warming: Why the “Wet-Get-Wetter, dry-get-drier” scaling does not hold over land. *Journal of Climate*, 28(20), 8078–8092. <https://doi.org/10.1175/JCLI-D-15-0369.1>

Deng, H., Pepin, N. C., & Chen, Y. (2017). Changes of snowfall under warming in the Tibetan Plateau. *Journal of Geophysical Research*, 122(14), 7323–7341. <https://doi.org/10.1002/2017JD026524>

Ding, B., Yang, K., Qin, J., Wang, L., Chen, Y., & He, X. (2014). The dependence of precipitation types on surface elevation and meteorological conditions and its parameterization. *Journal of Hydrology*, 513, 154–163. <https://doi.org/10.1016/j.jhydrol.2014.03.038>

Duan, A., & Xiao, Z. (2015). Does the climate warming hiatus exist over the Tibetan Plateau? *Scientific Reports*, 5, 1–9. <https://doi.org/10.1038/srep13711>

Flohn, H. (1957). Large-scale Aspects of the summer monsoon in South and east Asia. *Journal of the Meteorological Society of Japan. Ser. II*, 35(April), 180–186. https://doi.org/10.2151/jmsj1923.35A.0_180

Guan, X., Huang, J., Guo, R., & Lin, P. (2015). The role of dynamically induced variability in the recent warming trend slowdown over the Northern Hemisphere. *Scientific Reports*, 5, 12669. <https://doi.org/10.1038/srep12669>

He, Y., Tian, W., Huang, J., Wang, G., Ren, Y., Yan, H., et al. (2021). The mechanism of increasing summer water vapor over the Tibetan Plateau. *Journal of Geophysical Research: Atmospheres*, 126(10), 1–18. <https://doi.org/10.1029/2020JD034166>

Hersbach, H., Bell, B., Berrisford, P., Hirahara, S., Horányi, A., Muñoz-Sabater, J., et al. (2020). The ERA5 global reanalysis. *Quarterly Journal of the Royal Meteorological Society*, 146, 1999–2049. <https://doi.org/10.1002/qj.3803>

Huang, J., Chen, W., Wen, Z., Zhang, G., Li, Z., Zuo, Z., & Zhao, Q. (2019). Review of Chinese atmospheric science research over the past 70 years: Climate and climate change. *Science China Earth Sciences*, 62, 1514–1550. <https://doi.org/10.1007/s11430-019-9483-5>

Huang, J., Ma, J., Guan, X., Li, Y., & He, Y. (2019). Progress in semi-arid climate change studies in China. *Advances in Atmospheric Sciences*, 36(9), 922–937. <https://doi.org/10.1007/s00376-018-8200-9>

Kang, S. C., Xu, Y. W., You, Q. L., Flugel, W. A., Pepin, N., & Yao, T. D. (2010). Review of climate and cryospheric change in the Tibetan Plateau. *Environmental Research Letters*, 5(1), 015101. <https://doi.org/10.1088/1748-9326/5/1/015101>

Kobayashi, S., Ota, Y., Harada, Y., Ebina, A., Moriya, M., Onoda, H., et al. (2015). The JRA-55 reanalysis: General specifications and basic characteristics. *Journal of the Meteorological Society of Japan. Ser. II*, 93(1), 5–48. <https://doi.org/10.2151/jmsj.2015-001>

Lei, Y., Shi, J., Xiong, C., & Ji, D. (2021). Tracking the atmospheric-terrestrial water cycle over the Tibetan Plateau based on ERA5 and GRACE. *Journal of Climate*, 1–45. <https://doi.org/10.1175/JCLI-D-20-0692.1>

Li, F., Zhang, Y., Xu, Z., Teng, J., Liu, C., Liu, W., & Mpelasoka, F. (2013). The impact of climate change on runoff in the southeastern Tibetan Plateau. *Journal of Hydrology*, 505, 188–201. <https://doi.org/10.1016/j.jhydrol.2013.09.052>

Liu, C., & Allan, R. P. (2013). Observed and simulated precipitation responses in wet and dry regions 1850–2100. *Environmental Research Letters*, 8(3), 034002. <https://doi.org/10.1088/1748-9326/8/3/034002>

Liu, X., Xu, Z., Yang, H., & Vaghefi, S. A. (2021). Responses of the glacier mass balance to climate change in the Tibetan Plateau during 1975–2013. *Journal of Geophysical Research: Atmospheres*, 126(7), 1–14. <https://doi.org/10.1029/2019JD032132>

Loomis, B. D., Luthcke, S. B., & Sabaka, T. J. (2019). Regularization and error characterization of GRACE mascons. *Journal of Geodesy*, 93, 1381–1398. <https://doi.org/10.1007/s00190-019-01252-z>

Lu, C., Yu, G., & Xie, G. (2005). Tibetan plateau serves as a water tower. *International Geoscience and Remote Sensing Symposium (IGARSS)*, 5, 3120–3123. <https://doi.org/10.1109/IGARSS.2005.1526498>

Luo, J., Chen, H., & Zhou, B. (2020). Comparison of snowfall variations over China identified from different snowfall/rainfall discrimination methods. *Journal of Meteorological Research*, 34, 1114–1128. <https://doi.org/10.1007/s13351-020-0004-z>

Meng, F., Su, F., Li, Y., & Tong, K. (2019). Changes in terrestrial water storage during 2003–2014 and possible causes in Tibetan Plateau. *Journal of Geophysical Research: Atmospheres*, 124(6), 2909–2931. <https://doi.org/10.1029/2018JD029552>

Murray, F. W. (1967). On the computation of saturation vapor pressure. *Journal of Applied Meteorology and Climatology*, 6(1), 2032–2204. [https://doi.org/10.1175/1520-0450\(1967\)006<203:otcosy>2.0.co;2](https://doi.org/10.1175/1520-0450(1967)006<203:otcosy>2.0.co;2)

Neckel, N., Kropáček, J., Bolch, T., & Hochschild, V. (2014). Glacier mass changes on the Tibetan Plateau 2003–2009 derived from ICESat laser altimetry measurements. *Environmental Research Letters*, 9(1), 014009. <https://doi.org/10.1088/1748-9326/9/1/014009>

Onogi, K., Koide, H., Sakamoto, M., Kobayashi, S., Tsutsumi, J., Hatushika, H., et al. (2005). JRA-25: Japanese 25-year re-analysis project—Progress and status. *Quarterly Journal of the Royal Meteorological Society*, 131(613), 3259–3268. <https://doi.org/10.1256/qj.05.88>

Prein, A. F., & Heymsfield, A. J. (2020). Increased melting level height impacts surface precipitation phase and intensity. *Nature Climate Change*, 10(8), 771–776. <https://doi.org/10.1038/s41558-020-0825-x>

Pruppacher, H. R., & Klett, J. D. (2012). *Microphysics of clouds and precipitation*. Springer Science, Business Media. <https://doi.org/10.1007/978-0-306-48100-0>

Rangwala, I., Miller, J. R., & Xu, M. (2009). Warming in the Tibetan Plateau: Possible influences of the changes in surface water vapor. *Geophysical Research Letters*, 36(6), 1–6. <https://doi.org/10.1029/2009GL037245>

Rodell, M., Famiglietti, J. S., Wiese, D. N., Reager, J. T., Beaudoin, H. K., Landerer, F. W., & Lo, M. H. (2018). Emerging trends in global freshwater availability. *Nature*, 557(7707), 651–659. <https://doi.org/10.1038/s41586-018-0123-1>

Save, H., Bettadpur, S., & Tapley, B. D. (2016). High resolution CSR GRACE RL05 mascons. *Journal of Geophysical Research: Solid Earth*, 121, 7547–7569. <https://doi.org/10.1002/2016JB013007>

Simmons, A. J., & Burridge, D. M. (1981). An energy and angular-momentum conserving vertical finite-difference scheme and hybrid vertical coordinates. *Monthly Weather Review*, 109(4), 7582–7766. [https://doi.org/10.1175/1520-0493\(1981\)109<7582:aeamc>2.0.co;2](https://doi.org/10.1175/1520-0493(1981)109<7582:aeamc>2.0.co;2)

Song, C., Sheng, Y., Zhan, S., Wang, J., Ke, L., & Liu, K. (2020). Impact of amplified evaporation due to lake expansion on the water budget across the inner Tibetan Plateau. *International Journal of Climatology*, 40(4), 2091–2105. <https://doi.org/10.1002/joc.6320>

Su, F., Zhang, L., Ou, T., Chen, D., Yao, T., Tong, K., & Qi, Y. (2016). Hydrological response to future climate changes for the major upstream river basins in the Tibetan Plateau. *Global and Planetary Change*, 136, 82–95. <https://doi.org/10.1016/j.gloplacha.2015.10.012>

Sun, J., Yang, K., Guo, W., Wang, Y., He, J., & Lu, H. (2020). Why has the inner Tibetan plateau become wetter since the Mid-1990s? *Journal of Climate*, 33(19), 8507–8522. <https://doi.org/10.1175/JCLI-D-19-0471.1>

Wang, J., Zhang, M., Wang, S., Ren, Z., Che, Y., Qiang, F., & Qu, D. (2016). Decrease in snowfall/rainfall ratio in the Tibetan Plateau from 1961 to 2013. *Journal of Geographical Sciences*, 26(9), 1277–1288. <https://doi.org/10.1007/s11442-016-1326-8>

Wang, X., Tolksdorf, V., Otto, M., & Scherer, D. (2021). WRF-based dynamical downscaling of ERA5 reanalysis data for High Mountain Asia: Towards a new version of the High Asia refined analysis. *International Journal of Climatology*, 41, 743–762. <https://doi.org/10.1002/joc.6686>

Watkins, M. M., Wiese, D. N., Yuan, D.-N., Boening, C., & Landerer, F. W. (2015). Improved methods for observing Earth's time variable mass distribution with GRACE using spherical cap mascons. *Journal of Geophysical Research: Solid Earth*, 120, 2648–2671. <https://doi.org/10.1002/2014JB011547>

Wilson, W. T. (1941). Eos, Transactions American Geophysical Union. *Eos Trans. AGU*, 22(1), 182–195. <https://doi.org/10.1029/TR0221001p00182>

Wu, G., Liu, Y., He, B., Bao, Q., Duan, A., & Jin, F. F. (2012). Thermal controls on the asian summer monsoon. *Scientific Reports*, 2, 1–7. <https://doi.org/10.1038/srep00404>

Xu, K., Zhong, L., Ma, Y., Zou, M., & Huang, Z. (2020). A study on the water vapor transport trend and water vapor source of the Tibetan Plateau. *Theoretical and Applied Climatology*, 140(3–4), 1031–1042. <https://doi.org/10.1007/s00704-020-03142-2>

Xu, X., Lu, C., Shi, X., & Gao, S. (2008). World water tower: An atmospheric perspective. *Geophysical Research Letters*, 35(20), 1–5. <https://doi.org/10.1029/2008GL035867>

Xu, X., Zhao, T., Lu, C., Guo, Y., Chen, B., Liu, R., et al. (2014). An important mechanism sustaining the atmospheric water tower over the Tibetan Plateau. *Atmospheric Chemistry and Physics Discussions*, 14(12), 18255–18275. <https://doi.org/10.5194/acpd-14-18255-2014>

Yang, D., Ding, M., Dou, T., Han, W., Liu, W., Zhang, J., et al. (2021). On the differences in precipitation type between the arctic, Antarctica and Tibetan Plateau. *Frontiers of Earth Science*, 9, 607487. <https://doi.org/10.3389/feart.2021.607487>

Yang, K., Wu, H., Qin, J., Lin, C., Tang, W., & Chen, Y. (2014). Recent climate changes over the Tibetan Plateau and their impacts on energy and water cycle: A review. *Global and Planetary Change*, 112, 79–91. <https://doi.org/10.1016/j.gloplacha.2013.12.001>

Yao, T., Thompson, L., Yang, W., Yu, W., Gao, Y., Guo, X., et al. (2012). Different glacier status with atmospheric circulations in Tibetan Plateau and surroundings. *Nature Climate Change*, 2(9), 663–667. <https://doi.org/10.1038/nclimate1580>

Yao, T., Wu, F., Ding, L., Sun, J., Zhu, L., Piao, S., et al. (2015). Multispherical interactions and their effects on the Tibetan plateau's earth system: A review of the recent researches. *National Science Review*, 2(4), 468–488. <https://doi.org/10.1093/nsr/nwv070>

Yao, T., Xue, Y., Chen, D., Chen, F., Thompson, L., Cui, P., et al. (2019). Recent third pole's rapid warming accompanies cryospheric melt and water cycle intensification and interactions between monsoon and environment: Multidisciplinary approach with observations, modeling, and analysis. *Bulletin of the American Meteorological Society*, 100(3), 423–444. <https://doi.org/10.1175/BAMS-D-17-0057.1>

Zhang, G., Luo, W., Chen, W., & Zheng, G. (2019). A robust but variable lake expansion on the Tibetan Plateau. *Science Bulletin*, 64(18), 1306–1309. <https://doi.org/10.1016/j.scib.2019.07.018>

Zhang, G., Yao, T., Xie, H., Yang, K., Zhu, L., Shum, C. K., et al. (2020). Response of Tibetan Plateau lakes to climate change: Trends, patterns, and mechanisms. *Earth-Science Reviews*, 208, 103269. <https://doi.org/10.1016/j.earscirev.2020.103269>

Zhou, T., & Zhang, W. (2021). Anthropogenic warming of Tibetan Plateau and constrained future projection. *Environmental Research Letters*, 16(4), 044039. <https://doi.org/10.1088/1748-9326/abede8>

Zhu, X., Wu, T., Li, R., Wang, S., Hu, G., Wang, W., et al. (2017). Characteristics of the ratios of snow, rain and sleet to precipitation on the Qinghai-Tibet Plateau during 1961–2014. *Quaternary International*, 444, 137–150. <https://doi.org/10.1016/j.quaint.2016.07.030>